Lazar and Po
Journal of Materials Science: Materials Theory (2024) 8:5
https://doi.org/10.1186/s41313-024-00057-7

Journal of Materials Science: Materials Theory

RESEARCH Open Access

Non-singular straight dislocations in anisotropic crystals

Markus Lazar[1*] and Giacomo Po[2]

*Correspondence: markus.lazar@kit.edu

[1] Karlsruhe Institute of Technology (KIT), Institute of Engineering Mechanics, 76131 Karlsruhe, Germany
[2] Mechanical & Aerospace Engineering, University of Miami, Coral Gables, 33146 Florida, USA

Abstract

A non-singular dislocation theory of straight dislocations in anisotropic crystals is derived using simplified anisotropic incompatible first strain gradient elasticity theory. Based on the non-singular theory of dislocations for anisotropic crystals, all dislocation key-formulas of straight dislocations are derived in generalized plane strain, for the first time. In this model, the singularity of the dislocation fields at the dislocation core is regularized owing to the nonlocal nature of strain gradient elasticity. The non-singular dislocation fields of straight dislocations are obtained in terms of two-dimensional anisotropic Green functions of simplified anisotropic strain gradient elasticity. All necessary Green functions, including the two-dimensional Green tensor of the twofold anisotropic Helmholtz-Navier operator and the two-dimensional $\boldsymbol{F}$-tensor of generalized plane strain, are derived as sum of the classical part and a gradient part in terms of Meijer G-functions. Among others, we calculate the regularization of the Barnett solution for the elastic distortion of straight dislocations in an anisotropic crystal. In the framework of simplified anisotropic first strain gradient elasticity, the necessary material parameters are computed for cubic materials including aluminum (Al), copper (Cu), iron (Fe) and tungsten (W) using a second nearest-neighbour modified embedded-atom-method interatomic potential. The elastic distortion and stress fields of screw and edge dislocations of $\frac{1}{2}\langle 111\rangle$ Burgers vector in bcc iron and bcc tungsten and screw and edge dislocations of $\frac{1}{2}\langle 110\rangle$ Burgers vector in fcc copper and fcc aluminum have been computed and presented in contour plots.

Keywords: Anisotropic elasticity, Gradient elasticity, Nonlocality, Dislocations, Green tensor, Generalized plane strain

Introduction

This paper is dedicated to *Professor Nasr Ghoniem*, and it celebrates his illustrious and exemplary career in the field of the mechanics and physics of defects in crystals. His holistic research style, often involving experiments, theory, and numerical modeling, has created many valuable opportunities to connect researchers in the field. Our collaboration started about ten years ago, and it stemmed from an attempt to include characteristic length scales in the elastic theory of dislocations. Strengthened by several mutual visits between UCLA and TU Darmstadt, such collaboration led to several manuscripts (Po et al. 2014; Lazar and Po 2014, 2015a, b; Seif et al. 2015; Po et al. 2018; Lazar and Po 2018a, b; Po et al. 2019; Cui et al. 2019; Lazar et al. 2020). The present work

builds on our simplified strain gradient elasticity theory of dislocations in anisotropic crystals, and it derives specialized results for straight dislocations.

Classical continuum theories like the theory of linear elasticity are intrinsically size independent. For the study of dislocations in anisotropic crystals, classical anisotropic elasticity theory is often used (e.g., Bacon et al. (1980); Ting (1996); Hirth and Lothe (1982); Steeds (1973)). In two-dimensional (2D) anisotropic elasticity, the displacement fields of straight dislocations were derived by Stroh (1958, 1962) using the so-called Stroh formalism (see also Ting (1996)) and by Asaro et al. (1973) using the so-called integral formalism (see also Bacon et al. (1980); Balluffi (2012)). The integral formalism was originally derived from the Stroh formalism by Barnett and Lothe (1973). In two dimensions (2D), the elastic distortion and the strain energy of infinitely long straight dislocation lines with Burgers vector $\boldsymbol{b}$ in an anisotropic medium were given by Barnett and Swanger (1971). Using the two-dimensional anisotropic Green tensor of generalized plane strain, a Burgers-like formula for straight dislocations has been given by Lazar (2021) leading to a new derivation of the integral formalism (see also Lazar and Kirchner (2021)). It is well-known that classical anisotropic elasticity is not valid at small scales leading to singularities in the dislocation fields at the dislocation core. However, the near-field behaviour of the dislocation fields is of high importance for applications and for the understanding of physics within the dislocation core.

Dislocations are lattice defects of great significance, since they cause plasticity and hardening in crystals. A dislocation is a line defect in a crystal breaking locally the translational symmetry of the perfect crystal and leading in this way to a lower symmetry at the defect region of the imperfect crystal, namely at the dislocation core. In fact, the dislocation core is just an arrangement of atoms without any crystal symmetry. From the crystallographic point of view, the translational symmetry of crystals is disturbed by the lattice defect (dislocation) so that the symmetry of the point group of the dislocation core region is lower than the symmetry of the original point group of the perfect crystal. The broken symmetry in the dislocation core is important for many physical phenomena like plastic deformation, superalloys at high temperature, and birefringence (see, e.g., Kosevich (1979)). However, in some cases, it can be useful to look at the imperfect crystal from the point of view of approximate symmetry. Moreover, crystals have a discrete structure. The range of interaction can never be less than the discrete length, which is a finite length proportional to the lattice constant. Discreteness itself gives rise to nonlocality.

Therefore, a generalized continuum field theory, which possesses nonlocality and avoids singularities at small scales, is needed for an improved modelling of dislocations in crystals. Generalized continuum theories such as strain gradient elasticity and nonlocal elasticity are theories valid down to the Ångström-scale (see, e.g., Eringen (2002); Lazar (2017); Lazar et al. (2020, 2022)). Mindlin (1964) (see also Mindlin (1968)) derived the theory of compatible first strain gradient elasticity. Compatible first strain gradient elasticity incorporates the first gradient of the elastic strain tensor in the elastic energy in addition to the elastic strain tensor. For the isotropic case, this framework is characterized by the two Lamé constants and five strain gradient parameters leading to two characteristic lengths. In the early days of strain gradient elasticity, several trials (e.g., Lardner (1971); Rogula (1973)) to find non-singular fields produced by dislocations

were not successful, leading only to additional singularities in the dislocation fields. More than three decades later, Altan and Aifantis (1997) derived a simplified version of Mindlin's first strain gradient elasticity. Using such a simplified first strain gradient elasticity theory with only one characteristic length scale parameter, Gutkin and Aifantis (1996, 1997) found, for the first time, non-singular elastic strain fields of screw and edge dislocations in the framework of gradient elasticity. Lazar and Maugin (2005) (see also Lazar et al. (2005); Lazar (2017)) have shown how non-singular stress and strain fields of screw and edge dislocations can be computed in simplified first strain gradient elasticity including eigenstrain fields called simplified incompatible strain gradient elasticity. Such simplified first strain gradient elasticity is a particular version of Mindlin's first strain gradient elasticity where the double stress tensor can be expressed in terms of the gradient of the Cauchy stress tensor (see, e.g., Lazar and Maugin (2005); Lazar (2016)). Simplified incompatible strain gradient elasticity (gradient elasticity of Helmholtz type) provides robust non-singular solutions including one length scale parameter for the elastic distortion, plastic distortion, stress and displacement fields of screw and edge dislocations. An important mathematical property of simplified strain gradient elasticity is that it provides a straightforward regularization based on partial differential equations (PDEs) of higher order where the characteristic length scale parameter plays the role of a regularization parameter. The non-singular expressions of all dislocation key equations were given by Lazar (2012, 2013, 2014) for dislocation loops using simplified strain gradient elasticity. For dislocations, the incompatible version of simplified strain gradient elasticity including plastic distortion and dislocation density tensors is used leading to an incompatible strain gradient elasticity of defects. These non-singular dislocation key equations (Burgers formula, Mura-Willis equation and Peach-Koehler stress formula) have been implemented in the UCLA Discrete Dislocation Dynamics (DD) code called "model" (Model 2014) and used for applications (Po et al. 2014).

In order to model dislocations in cubic crystals, the extension of isotropic simplified incompatible strain gradient elasticity towards anisotropic simplified incompatible strain gradient elasticity has been given by Lazar and Po (2015a, b). Anisotropic incompatible strain gradient elasticity represents an anisotropic gradient elasticity with separable weak non-locality which is a special version of Mindlin's anisotropic strain gradient elasticity theory with up to six independent length scale parameters. The framework models materials where anisotropy is twofold, namely the bulk material anisotropy (far-field anisotropy) and a weak non-local anisotropy (near-field anisotropy) relevant at the Ångström-scale. Using Fourier transform, Lazar and Po (2015a, b) have computed the three-dimensional elastic Green tensor of anisotropic incompatible strain gradient elasticity as fundamental solution of the twofold anisotropic Helmholtz-Navier operator as integral over the unit sphere in Fourier space. Using anisotropic incompatible strain gradient elasticity, Po et al. (2018) have developed a non-singular theory of three-dimensional dislocation loops in anisotropic crystals. The theory is systematically developed as a generalization of the classical anisotropic elasticity theory of dislocation. The non-singular version of all key equations of anisotropic dislocation theory have been derived as line integrals in terms of the three-dimensional elastic Green tensor, including the Burgers displacement equation with isolated solid angle, the Peach-Koehler stress equation, the Mura-Willis equation for the elastic distortion, and the Peach-Koehler force.

The anisotropic non-singular dislocation theory is shown to be in good agreement with molecular statics calculations without fitting parameters, and unlike its singular counterpart, the sign of stress components does not show reversal as the core is approached. In particular, the virial stress of an edge dislocation in α-iron obtained from atomistic calculations is in perfect agreement with the non-singular stress using anisotropic incompatible strain gradient elasticity. Furthermore, the theory of anisotropic incompatible strain gradient elasticity has been used by Seif et al. (2015) to model the atomistically enabled non-singular anisotropic elastic representation of near-core dislocation stress fields in α-iron. Using a magnetic bond-order potential to model atomic interactions in iron, molecular statics calculations have been performed, and an optimization procedure has been developed to extract the required length scale parameter. Results showed that the method can accurately replicate the magnitude and decay of the near-core dislocation stresses even for atoms belonging to the dislocation core itself. Comparisons with the singular isotropic elasticity and anisotropic elasticity theories have shown that the non-singular anisotropic gradient elasticity theory of dislocations leads to a substantially more accurate representation of the stresses of both screw and edge dislocations near the dislocation core, in some cases showing improvements in accuracy of up to an order of magnitude. Therefore, as shown by Po et al. (2018) and Seif et al. (2015) results for dislocations in anisotropic crystals obtained by using anisotropic incompatible strain gradient elasticity theory are in agreement with atomistic results. The main advantage of those dislocation key-formulas is the absence of any singularity and that they are valid even in the dislocation core region. Until now, for non-singular fields of straight dislocations in anisotropic crystals the three-dimensional dislocation-key equations and the three-dimensional elastic Green tensor have been applied using the projection from 3D to 2D. However, the two-dimensional elastic Green tensor and the analytical expressions of straight dislocations are still lacking in the literature of anisotropic strain gradient elasticity.

What about dislocations in Mindlin's first strain gradient elasticity? For the incompatible version of Mindlin's first strain gradient elasticity, the two Lamé constants and the five strain gradient parameters lead to four characteristic lengths due to the presence of the eigenstrain fields of dislocations. Using the incompatible version of Mindlin's first strain gradient elasticity, non-singular and smooth displacement fields of screw and edge dislocations have been given by Delfani and Tavakol (2019) and Delfani et al. (2020), respectively. All non-singular dislocation fields including elastic strain, stress, and displacement fields of screw and edge dislocations have been computed by Lazar (2021) in the framework of incompatible first strain gradient elasticity of Mindlin type. The elastic fields of screw and edge dislocations have a similar form in simplified incompatible first strain gradient elasticity and in incompatible first strain gradient elasticity of Mindlin type (see, e.g., Lazar (2021, 2022)). Only the shape of the dislocation core of an edge dislocation with asymmetric form due to its inherent asymmetry can be modelled more realistic in incompatible first strain gradient elasticity of Mindlin type (Lazar 2021). Somehow, incompatible first strain gradient elasticity of Mindlin type is more sophisticated than simplified incompatible first strain gradient elasticity. For the isotropic case and the anisotropic case, the stress fields of straight dislocations and dislocation loops computed in the framework of simplified incompatible first strain gradient elasticity

are in full agreement with the corresponding stress fields obtained in Eringen's nonlocal elasticity of Helmholtz type (see, e.g., Eringen (2002); Lazar et al. (2005, 2020)). Thus, simplified incompatible first strain gradient elasticity is a very robust and powerful theory for an efficient modelling of dislocation fields without singularities at small scales. Moreover, the importance of simplified first strain gradient elasticity as non-singular dislocation continuum theory in comparison with other existing non-singular dislocation continuum theories has been given in Lazar (2017) and Po et al. (2014). Moreover, the use of nonlocality to describe the elastic fields within defect cores has received a renewed attention (e.g., Lazar and Agiasofitou (2011); Taupin et al. (2014, 2017); Lazar et al. (2020)). Zhang et al. (2016) considered the effects of core-spreading dislocation in anisotropic bi-materials. Semicoherent heterophase interfaces with core-spreading dislocation structures in magneto-electro-elastic multilayers under external surface loads were investigated in Vattré and Pan (2019).

The purpose of the present work is to derive the non-singular dislocation key-formulas of straight dislocations in an anisotropic medium using non-singular two-dimensional Green functions of simplified anisotropic first strain gradient elasticity. In A non-singular dislocation theory based on anisotropic incompatible strain gradient elasticity section, we review the framework of a non-singular dislocation theory based on anisotropic incompatible strain gradient elasticity. All necessary Green functions, including the two-dimensional Green tensor of the twofold anisotropic Helmholtz-Navier and the two-dimensional $\boldsymbol{F}$-tensor of generalized plane strain, are derived in Relevant Green functions in non-singular dislocation theory section. In Dislocation key-equations section, the dislocation key-equations of straight dislocations are computed for generalized plane strain. In Straight dislocations in cubic materials section, the dislocation fields of straight dislocations in cubic materials are given using simplified anisotropic first strain gradient elasticity. The necessary material parameters are given for cubic materials such as aluminum (Al), copper (Cu), iron (Fe) and tungsten (W) computed from a second nearest-neighbour modified embedded-atom-method (2NN MEAM) interatomic potential in Material parameters for cubic crystals section. The characteristic length scale of simplified anisotropic first strain gradient elasticity is computed based on the material parameters computed from a 2NN MEAM interatomic potential. As an application, the non-singular elastic fields of screw and edge dislocations of $\frac{1}{2}\langle 111\rangle$ Burgers vector in bcc iron and bcc tungsten and screw and edge dislocations of $\frac{1}{2}\langle 110\rangle$ Burgers vector in fcc copper and fcc aluminum are computed and presented in equal-value contour plots in Elastic distortion and stress fields of screw and edge dislocations in cubic crystals section. Some technical remarks are given in the Appendix.

A non-singular dislocation theory based on anisotropic incompatible strain gradient elasticity

Here, we consider the eigendistortion problem of dislocations in an anisotropic crystal. We consider an infinite elastic body in three-dimensional space and use the property that the gradient of the displacement field $\boldsymbol{u}$ can be additively decomposed into an incompatible elastic distortion tensor $\boldsymbol{\beta}$ and an incompatible plastic distortion (eigendistortion) tensor $\boldsymbol{\beta}^{\mathrm{P}}$:

$$\partial_j u_i = \beta_{ij} + \beta^{\mathrm{P}}_{ij}\,, \qquad i,j = 1,2,3\,. \tag{1}$$

The elastic strain tensor, $\boldsymbol{e}$, is the symmetric part of $\boldsymbol{\beta}$:

$$e_{ij} = \frac{1}{2}\left(\beta_{ij} + \beta_{ji}\right). \tag{2}$$

In dislocation theory, the dislocation density tensor, $\boldsymbol{\alpha}$, is defined in terms of the incompatible plastic distortion tensor (see, e.g., Kröner (1958); deWit (1973a); Lazar (2014))

$$\alpha_{ij} = -\epsilon_{jkl}\partial_k \beta^{\mathrm{P}}_{il} \tag{3}$$

and can be also expressed in terms of the incompatible elastic distortion tensor

$$\alpha_{ij} = \epsilon_{jkl}\partial_k \beta_{il}\,, \tag{4}$$

where ϵ_{jkl} indicates the Levi-Civita tensor. Sometimes, the tensor $\boldsymbol{\alpha}$ is called the Kröner-Nye tensor. Moreover, the dislocation density tensor satisfies the Bianchi identity of dislocations

$$\partial_j \alpha_{ij} = 0\,, \tag{5}$$

which means that dislocations cannot end inside the body.

Mindlin's anisotropic first strain gradient elasticity

In Mindlin's anisotropic first strain gradient elasticity theory (Mindlin 1964, 1968, 1972), the strain energy density for a homogeneous and centrosymmetric[1] material is given by (see also Lazar and Kirchner (2007); Lazar et al. (2022))

$$\mathcal{W} = \frac{1}{2}\,\mathbb{C}_{ijkl} e_{ij} e_{kl} + \frac{1}{2}\,\mathbb{D}_{ijmkln}\partial_m e_{ij}\partial_n e_{kl}\,, \tag{6}$$

where $\mathbb{C}_{ijkl}$ is the fourth-rank constitutive tensor of elastic constants possessing the minor symmetries

$$\mathbb{C}_{ijkl} = \mathbb{C}_{jikl} = \mathbb{C}_{ijlk} \tag{7}$$

and the major symmetry

$$\mathbb{C}_{ijkl} = \mathbb{C}_{klij} \tag{8}$$

while $\mathbb{D}_{ijmkln}$ is the sixth-rank constitutive tensor of the gradient-elastic constants possesses the minor symmetries

$$\mathbb{D}_{ijmkln} = \mathbb{D}_{jimkln} = \mathbb{D}_{ijmlkn} \tag{9}$$

and the major symmetry

[1] Due to the centrosymmetry, there is no coupling between e_{ij} and $\partial_m e_{kl}$.

$$\mathbb{D}_{ijmkln} = \mathbb{D}_{klnijm} \,. \tag{10}$$

For the general anisotropic case (triclinic), the constitutive tensor $\mathbb{C}_{ijkl}$ has 21 independent elastic constants and the constitutive tensor $\mathbb{D}_{ijmkln}$ has 171 independent gradient-elastic constants (see, e.g., Auffray et al. (2013)). For cubic crystals of point group $m\bar{3}m$, the constitutive tensor $\mathbb{C}_{ijkl}$ has 3 independent elastic constants and the constitutive tensor $\mathbb{D}_{ijmkln}$ has 11 independent gradient-elastic constants (see, e.g., Mindlin (1968); Auffray et al. (2013); Lazar et al. (2022); Lazar and Agiasofitou (2023)).

Simplified anisotropic first strain gradient elasticity

In simplified anisotropic first strain gradient elasticity, it is assumed (see also Lazar and Kirchner (2007); Gitman et al. (2010); Lazar and Po (2015b); Po et al. (2018); Polizzotto (2018)) that the sixth-rank constitutive tensor $\mathbb{D}_{ijmkln}$ can be decomposed into the product of the fourth-rank constitutive tensor $\mathbb{C}_{ijkl}$ and a second-rank tensor Λ_{mn} of gradient length scale parameters with units of squared length, that is

$$\mathbb{D}_{ijmkln} = \mathbb{C}_{ijkl}\, \Lambda_{mn} \,. \tag{11}$$

Note that Eq. (11) represents the constitutive assumption of simplified anisotropic first strain gradient elasticity. As consequence of the major symmetry (10) and of positive definiteness of $\mathcal{W}$, the tensor Λ_{mn} must be symmetric and positive definite. The classification of the gradient length scale tensor Λ_{mn} for triclinic, monoclinic, orthorhombic, tetragonal, hexagonal, trigonal, cubic, and isotropic materials has been given in Lazar and Po (2015b); Lazar et al. (2020). For the general anisotropic case (triclinic), the gradient length scale tensor Λ_{mn} has 6 independent gradient length scale parameters. The decomposition (11) represents the separation of two anisotropies present in anisotropic strain gradient elasticity, namely the elastic bulk anisotropy (elastic moduli anisotropy) via $\mathbb{C}_{ijkl}$ and the anisotropy of the gradient length scale parameters (internal length anisotropy or weak nonlocal anisotropy at small scales) via Λ_{mn}. The latter, which is not present in classical anisotropic elasticity, reflects the discrete nature of matter and becomes relevant in the presence of defects at the Ångström-scale as dislocation core anisotropy. The decomposition (11) is not ad hoc because it considers that the gradients ∂_m and ∂_n in Eq. (6) give rise to length scale effects via Λ_{mn}. In general, the symmetries of the tensors $\mathbb{C}_{ijkl}$ and Λ_{mn} can be different due to the twofold anisotropy. Also note that the decomposition (11) in strain gradient elasticity corresponds to the twofold anisotropy present in Eringen's nonlocal elasticity theory, namely the elastic moduli anisotropy of the bulk described by $\mathbb{C}_{ijkl}$ and the anisotropy of the nonlocality at small scales described by a nonlocal kernel function α (see Eringen (1978, 2002); Lazar and Agiasofitou (2011); Lazar et al. (2020)). Such a twofold anisotropy can be used to model the anisotropy of the dislocation core in an anisotropic crystal (as mentioned in the Introduction), namely the symmetry of the perfect crystal via $\mathbb{C}_{ijkl}$ and the lower symmetry of the dislocation core of the imperfect crystal via Λ_{mn}.

Using Eq. (11), the strain energy density (6) reduces to

$$\mathcal{W} = \frac{1}{2}\,\mathbb{C}_{ijkl}e_{ij}e_{kl} + \frac{1}{2}\,\Lambda_{mn}\mathbb{C}_{ijkl}\,\partial_m e_{ij}\partial_n e_{kl}\,. \tag{12}$$

The Cauchy stress tensor $\boldsymbol{\sigma}$ and the double stress tensor $\boldsymbol{\tau}$ are given by

$$\sigma_{ij} = \frac{\partial \mathcal{W}}{\partial e_{ij}} = \mathbb{C}_{ijkl}e_{kl}\,, \tag{13}$$

$$\tau_{ijm} = \frac{\partial \mathcal{W}}{\partial(\partial_m e_{ij})} = \Lambda_{mn}\mathbb{C}_{ijkl}\partial_n e_{kl} = \Lambda_{mn}\partial_n\sigma_{ij}\,. \tag{14}$$

An important property of simplified strain gradient elasticity theory is the remarkable fact that the double stress tensor (14) is nothing but the first gradient of the Cauchy stress tensor (13) multiplied by the length scale tensor Λ_{mn} (see also Lazar and Maugin (2005)). This is the result of the decomposition (11). Using the constitutive relations (13) and (14), the strain energy density (12) can be written in the "compact" form

$$\mathcal{W} = \frac{1}{2}\,\sigma_{ij}e_{ij} + \frac{1}{2}\,\Lambda_{mn}(\partial_m\sigma_{ij})(\partial_n e_{ij}) \tag{15}$$

in terms of the stress tensor σ_{ij} and the elastic strain tensor e_{ij} and their first gradient. The strain energy density (15) has a remarkable symmetry in the stress and elastic strain tensors.

The condition of the static equilibrium is given by the Euler-Lagrange equation and reads as

$$\frac{\delta \mathcal{W}}{\delta u_i} := \frac{\partial \mathcal{W}}{\partial u_i} - \partial_j\,\frac{\partial \mathcal{W}}{\partial(\partial_j u_i)} + \partial_m\partial_j\,\frac{\partial \mathcal{W}}{\partial(\partial_m\partial_j u_i)} = 0\,. \tag{16}$$

In terms of the Cauchy stress and double stress tensors, Eq. (16) reduces to

$$\partial_j\big(\sigma_{ij} - \partial_m\tau_{ijm}\big) = 0\,. \tag{17}$$

Using Eq. (14), Eq. (17) simplifies to

$$L\partial_j\sigma_{ij} = 0\,, \tag{18}$$

where

$$L = 1 - \Lambda_{mn}\partial_m\partial_n \tag{19}$$

is a scalar anisotropic Helmholtz operator. Using Eqs. (1) and (13), Eq. (18) can be cast in the following twofold anisotropic inhomogeneous Helmholtz-Navier equation for the displacement vector

$$LL_{ik}u_k = \mathbb{C}_{ijkl}\partial_j L\beta^{\mathrm{P}}_{kl} \tag{20}$$

with the anisotropic Navier operator

$$L_{ik} = \mathbb{C}_{ijkl}\partial_j\partial_l\,. \tag{21}$$

The "source-term" in Eq. (20) is given by the plastic distortion tensor $\boldsymbol{\beta}^{\mathrm{P}}$. Equation (20) is an inhomogeneous partial differential equation of fourth order and can be written as system of two partial differential equations (Lazar 2014), namely an anisotropic inhomogeneous Helmholtz-Navier equation for the displacement vector $\boldsymbol{u}$:

$$LL_{ik}u_k = \mathbb{C}_{ijkl}\partial_j\beta^{\mathrm{P},0}_{kl}\,, \tag{22}$$

where the "source-term" in Eq. (22) is given by the classical plastic distortion tensor $\boldsymbol{\beta}^{\mathrm{P},0}$ and an inhomogeneous Helmholtz equation for the plastic distortion tensor $\boldsymbol{\beta}^{\mathrm{P}}$:

$$L\beta^{\mathrm{P}}_{kl} = \beta^{\mathrm{P},0}_{kl}\,. \tag{23}$$

Moreover, the dislocation density tensor (3) also satisfies an inhomogeneous Helmholtz equation

$$L\alpha_{kl} = \alpha^0_{kl}\,, \tag{24}$$

where $\boldsymbol{\alpha}^0$ denotes the classical dislocation density tensor.

Relevant Green functions in non-singular dislocation theory

In this section, all two-dimensional Green functions necessary in non-singular dislocation theory of straight dislocation are given.

Two-dimensional Green tensor of the twofold anisotropic Helmholtz-Navier operator

First, we derive the two-dimensional Green tensor of the twofold anisotropic Helmholtz-Navier Eq. (22) which is a partial differential equation of fourth order. The two-dimensional Green tensor of the twofold anisotropic Helmholtz-Navier operator LL_{ik} is defined by

$$LL_{ik}G_{kj}(\boldsymbol{x}) = -\delta_{ij}\delta(\boldsymbol{x})\,, \qquad i,j,k = 1,2,3\,, \tag{25}$$

where $\boldsymbol{x} \in \mathbb{R}^2$. In Eq. (25), δ_{ij} is the Kronecker symbol and $\delta(.)$ is the two-dimensional Dirac delta-function.

Since the Helmholtz-Navier operator LL_{ik} is the product of the Helmholtz operator L and the Navier operator L_{ik}, the corresponding Green tensor of the Helmholtz-Navier Eq. (25) can be written as the convolution of the Green function G^L of the anisotropic Helmholtz equation and the "classical" Green tensor G^0_{ij} of the anisotropic Navier operator, that is

$$G_{ij} = G^L * G^0_{ij} = G^0_{ij} * G^L \tag{26}$$

with G^L and G^0_{ij} satisfying, respectively:

$$LG^L(\boldsymbol{x}) = \delta(\boldsymbol{x})\,, \tag{27}$$

$$L_{ik}G^0_{kj}(\boldsymbol{x}) = -\delta_{ij}\delta(\boldsymbol{x})\,, \tag{28}$$

where the anisotropic Helmholtz operator L and the anisotropic Navier operator L_{ik} are given by

$$L = 1 - \Lambda_{mn}\partial_m\partial_n\,, \qquad m,n = 1,2 \tag{29}$$

$$L_{ik} = \mathbb{C}_{ijkl}\partial_j\partial_l\,, \qquad i,k = 1,2,3 \qquad j,l = 1,2\,. \tag{30}$$

Here $*$ denotes the spatial convolution and $\mathbf{\Lambda}$ is a symmetric 2×2 matrix:

$$\Lambda_{mn} = \begin{pmatrix} \Lambda_{11} & \Lambda_{12} \\ \Lambda_{12} & \Lambda_{22} \end{pmatrix}. \tag{31}$$

The corresponding inverse matrix $\mathbf{\Lambda}^{-1} = \operatorname{adj}\mathbf{\Lambda}/\det\mathbf{\Lambda}$ is given by

$$\Lambda^{-1}_{mn} = \frac{1}{\Lambda_{11}\Lambda_{22} - \Lambda_{12}^2}\begin{pmatrix} \Lambda_{22} & -\Lambda_{12} \\ -\Lambda_{12} & \Lambda_{11} \end{pmatrix}. \tag{32}$$

Equation (26) reveals that the Green function G^L plays the role of an anisotropic regularization function for the singular Green tensor of classical elasticity, G^0_{ij}. The two-dimensional anisotropic Green function G^L of Eq. (27) reads (see Lazar and Agiasofitou (2011); Lazar et al. (2020))

$$G^L(\boldsymbol{x}) = \frac{1}{2\pi}\,\frac{1}{\sqrt{\det\mathbf{\Lambda}}}\,K_0\Big(\sqrt{\boldsymbol{x}^T(\mathbf{\Lambda}^{-1})\boldsymbol{x}}\Big)\,, \tag{33}$$

where K_0 denotes the modified Bessel function of order 0. Notice that Eq. (33) possesses an independent anisotropy due to the tensor Λ_{mn} with 3 independent components Λ_{11}, Λ_{12}, Λ_{22} describing anisotropic length scale effects in the x_1x_2 plane. In order that Λ_{mn} with $m,n = 1,2$ is positive definite, it is necessary and sufficient that the following inequalities are satisfied (see Lazar and Agiasofitou (2011); Lazar and Po (2015b); Lazar et al. (2020))

$$\Lambda_{11} > 0\,, \qquad \det\mathbf{\Lambda} > 0\,. \tag{34}$$

The two-dimensional Green tensor of the Navier operator in classical anisotropic elasticity is given by Lazar (2021)

$$G^0_{ij}(\boldsymbol{x}) = -\frac{1}{4\pi^2}\int_0^{2\pi}\hat{L}^{-1}_{ij}(\boldsymbol{\kappa})\big[\gamma + \ln|\boldsymbol{\kappa}\cdot\boldsymbol{x}|\big]\,\mathrm{d}\phi\,, \tag{35}$$

where γ is the Euler constant ($\gamma \approx 0.57721\ldots$).

Solution using the method of Fourier transform

The two-dimensional Fourier transform of Eq. (25) gives for the Green tensor in Fourier space $\hat{G}_{kj}(\boldsymbol{k})$:

$$(1 + \Lambda_{mn}k_mk_n)\hat{L}_{ik}\hat{G}_{kj}(\boldsymbol{k}) = \delta_{ij}\,, \qquad \boldsymbol{k}\in\mathbb{R}^2\,, \tag{36}$$

where

$$\hat{L}_{ik}(\boldsymbol{k}) = \mathbb{C}_{ijkl} k_j k_l \,, \qquad i,k = 1,2,3 \qquad j,l = 1,2 \tag{37}$$

is the Navier operator in Fourier space. Now, if we define the two-dimensional unit vector

$$\boldsymbol{\kappa} = \frac{\boldsymbol{k}}{k} \,, \qquad k = \sqrt{k_1^2 + k_2^2} \,, \qquad \boldsymbol{\kappa}^2 = 1 \,, \tag{38}$$

then the solution of Eq. (36) in Fourier space is given by

$$\begin{aligned} \hat{G}_{ij}(\boldsymbol{k}) &= \frac{1}{k^2} \frac{1}{1 + k^2 \Lambda_{mn} \kappa_m \kappa_n} \hat{L}_{ij}^{-1}(\boldsymbol{\kappa}) \\ &= \frac{1}{k^2} \frac{1}{1 + \lambda^2(\boldsymbol{\kappa})\, k^2} \hat{L}_{ij}^{-1}(\boldsymbol{\kappa}) \,. \end{aligned} \tag{39}$$

In Eq. (39), we have introduced the function $\lambda(\boldsymbol{\kappa})$

$$\lambda(\boldsymbol{\kappa}) = \sqrt{\Lambda_{mn} \kappa_m \kappa_n} \,, \qquad m,n = 1,2 \,. \tag{40}$$

The two-dimensional Green tensor in real space is obtained by the two-dimensional inverse Fourier transform of Eq. (39)

$$\begin{aligned} G_{ij}(\boldsymbol{x}) &= \frac{1}{4\pi^2} \int_{\mathbb{R}^2} \frac{\hat{L}_{ij}^{-1}(\boldsymbol{\kappa}) \, \cos(\boldsymbol{k} \cdot \boldsymbol{x})}{k^2 (1 + \lambda^2(\boldsymbol{\kappa})\, k^2)} \, \mathrm{d}\hat{V} \\ &= \frac{1}{4\pi^2} \int_0^{2\pi} \hat{L}_{ij}^{-1}(\boldsymbol{\kappa}) \int_0^{\infty} \frac{\cos(k\boldsymbol{\kappa} \cdot \boldsymbol{x})}{k(1 + \lambda^2(\boldsymbol{\kappa})\, k^2)} \, \mathrm{d}k \, \mathrm{d}\phi \\ &= \frac{1}{4\pi^2} \int_0^{2\pi} \hat{L}_{ij}^{-1}(\boldsymbol{\kappa}) \int_0^{\infty} \left(\frac{1}{k} - \frac{k}{k^2 + 1/\lambda^2(\boldsymbol{\kappa})} \right) \cos(k\boldsymbol{\kappa} \cdot \boldsymbol{x}) \, \mathrm{d}k \, \mathrm{d}\phi \,. \end{aligned} \tag{41}$$

In Eq. (41), $\mathrm{d}\hat{V} = k \, \mathrm{d}k \, \mathrm{d}\phi$ indicates the two-dimensional volume element in Fourier space in polar coordinates, and ϕ $(0 < \phi \leq 2\pi)$ is an appropriate polar angle scanning a unit circle $\boldsymbol{\kappa}^2 = 1$. The two-dimensional unit vector $\boldsymbol{\kappa}(\phi)$ varies with ϕ and can be expressed as

$$\boldsymbol{\kappa}(\phi) = \cos\phi \, \hat{\boldsymbol{e}}_1 + \sin\phi \, \hat{\boldsymbol{e}}_2 \,, \tag{42}$$

where the unit vectors $\hat{\boldsymbol{e}}_1$ and $\hat{\boldsymbol{e}}_2$ represent a Cartesian basis in the two dimensional plane.[2]

Integration in k is performed using the relations

$$\int_0^{\infty} \frac{1}{k} \cos(k \, \boldsymbol{\kappa} \cdot \boldsymbol{x}) \, \mathrm{d}k = -\gamma - \ln|\boldsymbol{\kappa} \cdot \boldsymbol{x}| \tag{43}$$

and

$$\int_0^{\infty} \frac{k}{k^2 + 1/\lambda^2} \cos(k \, \boldsymbol{\kappa} \cdot \boldsymbol{x}) \, \mathrm{d}k = \frac{\sqrt{\pi}}{2} \, G_{1,3}^{2,1}\left(\frac{(\boldsymbol{\kappa} \cdot \boldsymbol{x})^2}{4\lambda^2} \middle| \begin{matrix} 0 \\ 0, \, 0, \, \frac{1}{2} \end{matrix} \right) , \tag{44}$$

[2] In the numerical evaluation of integrals over the unit circle it is convenient to consider a local reference system such that $\hat{\boldsymbol{e}}_1 = \boldsymbol{x}/\|\boldsymbol{x}\|$.

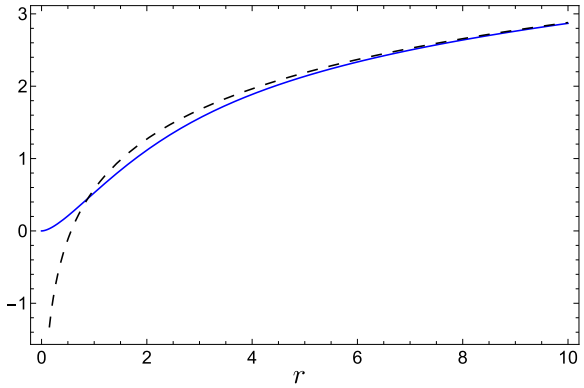

Fig. 1 Plot of the integrand of the Green tensor (45) (blue line) and classical logarithmic singularity (dashed line) with $r = (\boldsymbol{\kappa} \cdot \boldsymbol{x})$ and $\lambda = 1$

where $G^{a,b}_{c,d}()$ is the Meijer G-function (see Erdélyi et al. (1981); Gradshteyn and Ryzhik (2000)). Hence, Eq. (41) can be expressed as:

$$G_{ij}(\boldsymbol{x}) = -\frac{1}{4\pi^2}\int_0^{2\pi} \hat{L}^{-1}_{ij}(\boldsymbol{\kappa})\left[\gamma + \ln|\boldsymbol{\kappa}\cdot\boldsymbol{x}| + \frac{\sqrt{\pi}}{2}\, G^{2,1}_{1,3}\left(\frac{(\boldsymbol{\kappa}\cdot\boldsymbol{x})^2}{4\lambda^2(\boldsymbol{\kappa})}\,\middle|\, \begin{matrix} 0 \\ 0,\ 0,\ \frac{1}{2}\end{matrix}\right)\right] \mathrm{d}\phi\,. \tag{45}$$

It can be seen that the Green tensor (45) of the Helmholtz-Navier operator is a sum of the Green tensor (35) of the Navier operator and a gradient part given in terms of the Meijer G-function. The two-dimensional Green tensor (45) is an integral over the unit circle in Fourier space, whereas the three-dimensional Green tensor is an integral over the unit sphere in Fourier space (see also Lazar and Po (2015b)).

The asymptotics of the Meijer G-function with the above values is

$$G^{2,1}_{1,3}\left(z\,\middle|\, \begin{matrix} 0 \\ 0,\ 0,\ \frac{1}{2}\end{matrix}\right) \approx -\frac{1}{\sqrt{\pi}}\left(\gamma - \psi^{(0)}(1/2) + \ln z\right) + \mathcal{O}(z) \quad \text{for} \quad z \ll 1\,, \tag{46}$$

where $z = \frac{(\boldsymbol{\kappa}\cdot\boldsymbol{x})^2}{4\lambda^2(\boldsymbol{\kappa})}$ and $\psi^{(0)}$ is the digamma function. The logarithmic singularity of the Green tensor (35) of the Navier operator is removed (regularized) in the Green tensor (45) of the Helmholtz-Navier operator by the near field of the Meijer G-function (see Eq. (46)). The integrand (bracket) of Eq. (45) is plotted in Fig. 1. Therefore, the integrand of the Green tensor (45) of the Helmholtz-Navier operator is finite and non-singular, namely

$$G_{ij}(\boldsymbol{0}) = \frac{1}{4\pi^2}\int_0^{2\pi} \hat{L}^{-1}_{ij}(\boldsymbol{\kappa}) \ln\left(1/\lambda(\boldsymbol{\kappa})\right) \mathrm{d}\phi\,. \tag{47}$$

The Meijer G-function in Eq. (45) can be expressed in terms of elementary functions, suitable for numerical manipulation and implementation, as

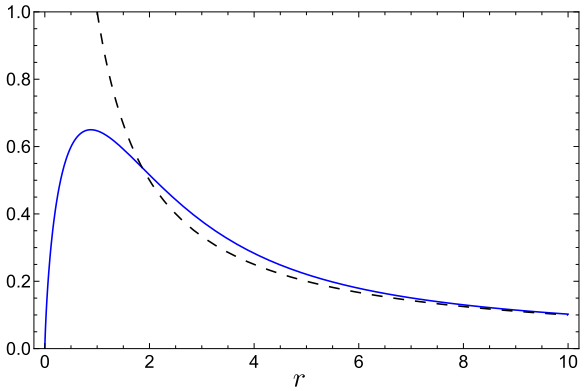

Fig. 2 Plot of the integrand of the gradient of the Green tensor, Eq. (51), (blue line) and classical $1/r$-singularity (dashed line) with $r = (\boldsymbol{\kappa} \cdot \boldsymbol{x})$ and $\lambda = 1$

$$G^{2,1}_{1,3}\left(z \middle| \begin{matrix} 0 \\ 0,\ 0,\ \frac{1}{2} \end{matrix}\right) = -\frac{2}{\sqrt{z}}\left[\mathrm{Chi}\left(2\sqrt{z}\right)\cosh\left(2\sqrt{z}\right) - \mathrm{Shi}\left(2\sqrt{z}\right)\sinh\left(2\sqrt{z}\right)\right], \tag{48}$$

where the hyperbolic sine integral function is given by

$$\mathrm{Shi}(z) = \int_0^z \sinh(t)/t \, \mathrm{d}t \tag{49}$$

and the hyperbolic cosine integral function is given by

$$\mathrm{Chi}(z) = \gamma + \ln(z) + \int_0^z (\cosh(t) - 1)/t \, \mathrm{d}t \, . \tag{50}$$

Note that $\mathrm{Chi}(z)$ has a branch cut discontinuity in the complex z plane running from $-\infty$ to 0, whereas $\mathrm{Shi}(z)$ has no branch cut discontinuity.

Given G_{ij} as an integral over the unit circle in Fourier space, its gradient is obtained as:

$$\begin{aligned} \partial_m G_{ij}(\boldsymbol{x}) = -\frac{1}{4\pi^2}\int_0^{2\pi} \hat{L}^{-1}_{ij}(\boldsymbol{\kappa})\,\frac{\kappa_m}{\boldsymbol{\kappa}\cdot\boldsymbol{x}} \\ \times\left[1 - \frac{\sqrt{\pi}\,(\boldsymbol{\kappa}\cdot\boldsymbol{x})^2}{4\lambda^2(\boldsymbol{\kappa})}\, G^{2,1}_{1,3}\left(\frac{(\boldsymbol{\kappa}\cdot\boldsymbol{x})^2}{4\lambda^2(\boldsymbol{\kappa})}\middle| \begin{matrix} -1 \\ -1,\ 0,\ -\frac{1}{2} \end{matrix}\right)\right]\mathrm{d}\phi \, . \end{aligned} \tag{51}$$

The asymptotics of the Meijer G-function with the above values are

$$G^{2,1}_{1,3}\left(z \middle| \begin{matrix} -1 \\ -1,\ 0,\ -\frac{1}{2} \end{matrix}\right) \approx \frac{1}{\sqrt{\pi}z} + \frac{2}{\sqrt{\pi}}\left(\gamma - \psi^{(0)}(3/2) + \ln z\right) + \mathcal{O}(z) \quad \text{for} \quad z \ll 1 \tag{52}$$

and

$$\sqrt{\pi}z\, G^{2,1}_{1,3}\left(z \middle| \begin{matrix} -1 \\ -1,\ 0,\ -\frac{1}{2} \end{matrix}\right) \approx 1 + 2\left(\gamma - \psi^{(0)}(3/2) + \ln z\right)z + \mathcal{O}(z^2) \, . \tag{53}$$

The "classical" $1/r$-singularity is removed (regularized) in the integrand of Eq. (51) due to the near field of the Meijer G-function (see Eq. (53)). Therefore, the integrand of Eq. (51) is non-singular, namely zero at the origin (see Fig. 2).

The Meijer G-function in Eq. (51) can be expressed in terms of elementary functions, suitable for numerical manipulation and implementation, as

$$\begin{aligned} G^{2,1}_{1,3}\left(z\left|\begin{matrix}-1\\ -1,\ 0,\ -\frac{1}{2}\end{matrix}\right.\right) &= \frac{1}{\sqrt{\pi z}} \\ &- \frac{2}{\sqrt{\pi z}}\left[\mathrm{Shi}\left(2\sqrt{z}\right)\cosh\left(2\sqrt{z}\right) - \mathrm{Chi}\left(2\sqrt{z}\right)\sinh\left(2\sqrt{z}\right)\right]. \end{aligned} \tag{54}$$

Two-dimensional *F*-tensor in strain gradient anisotropic elasticity

The so-called $\boldsymbol{F}$-tensor has been introduced by Kirchner (1984) (see also Lazar and Kirchner (2013); Po et al. (2018); Lazar et al. (2020)). The two-dimensional $\boldsymbol{F}$-tensor is defined by (see also Lazar (2021))

$$F_{mnij} = -\partial_m\partial_n G_{ij} * G^{\Delta}\,, \qquad i,j=1,2,3 \qquad m,n=1,2\,, \tag{55}$$

where the two-dimensional Green function of the Laplace operator reads (see, e.g., Vladimirov (1971))

$$\Delta G^{\Delta}(\boldsymbol{x}) = \delta(\boldsymbol{x}) \tag{56}$$

with

$$G^{\Delta} = \frac{1}{2\pi}\,\ln r\,, \tag{57}$$

where $r = \sqrt{x_1^2 + x_2^2}$.

Using the two-dimensional Fourier transform, Eq. (55) becomes

$$\hat{F}_{mnij}(\boldsymbol{k}) = \frac{1}{k^2}\,\frac{\kappa_m\kappa_n}{1+\lambda^2(\boldsymbol{\kappa})\,k^2}\,\hat{L}^{-1}_{ij}(\boldsymbol{\kappa})\,, \qquad i,j=1,2,3 \qquad m,n=1,2\,. \tag{58}$$

The two-dimensional inverse Fourier transform gives the two-dimensional $\boldsymbol{F}$-tensor

$$\begin{aligned} F_{mnij}(\boldsymbol{x}) = -\frac{1}{4\pi^2}\int_0^{2\pi} &\hat{L}^{-1}_{ij}(\boldsymbol{\kappa})\,\kappa_m\kappa_n \\ &\times\left[\gamma + \ln|\boldsymbol{\kappa}\cdot\boldsymbol{x}| + \frac{\sqrt{\pi}}{2}\,G^{2,1}_{1,3}\left(\frac{(\boldsymbol{\kappa}\cdot\boldsymbol{x})^2}{4\lambda^2(\boldsymbol{\kappa})}\,\middle|\,\begin{matrix}0\\ 0,\ 0,\ \frac{1}{2}\end{matrix}\right)\right]\mathrm{d}\phi\,. \end{aligned} \tag{59}$$

Therefore, the integrand of the $\boldsymbol{F}$-tensor (59) is finite and non-singular, namely

$$F_{mnij}(\boldsymbol{0}) = \frac{1}{4\pi^2}\int_0^{2\pi}\hat{L}^{-1}_{ij}(\boldsymbol{\kappa})\,\kappa_m\kappa_n\ln\left(1/\lambda(\boldsymbol{\kappa})\right)\mathrm{d}\phi\,. \tag{60}$$

From a numerical viewpoint, it is noteworthy that the Green tensor (45), its gradient (51), and the $\boldsymbol{F}$-tensor (59) are even functions of $\boldsymbol{k}$. Hence the integral over the unit circle appearing in their expressions can be expressed by twice the integral over a semicircle.

Two-dimensional Green function of the anisotropic Laplace-Helmholtz equation

The Green function of the anisotropic Laplace-Helmholtz equation is defined by

$$\Delta L G^{\Delta L}(\boldsymbol{x}) = \delta(\boldsymbol{x}) \tag{61}$$

and in Fourier space it becomes

$$\begin{aligned} \hat{G}^{\Delta L}(\boldsymbol{k}) &= -\frac{1}{k^2}\,\frac{1}{1+\lambda^2(\boldsymbol{\kappa})\,k^2} \\ &= -\frac{1}{k^2} + \frac{1}{k^2 + 1/\lambda^2(\boldsymbol{\kappa})}\,. \end{aligned} \tag{62}$$

Using the two-dimensional inverse Fourier transform, the Green function of the anisotropic Laplace-Helmholtz equation is obtained for general anisotropy

$$G^{\Delta L}(\boldsymbol{x}) = \frac{1}{2\pi}\,\ln r + \frac{\sqrt{\pi}}{8\pi^2}\int_0^{2\pi} G^{2,1}_{1,3}\left(\frac{(\boldsymbol{\kappa}\cdot\boldsymbol{x})^2}{4\lambda^2(\boldsymbol{\kappa})}\,\middle|\,\begin{matrix}0\\0,\ 0,\ \frac{1}{2}\end{matrix}\right)\mathrm{d}\phi \tag{63}$$

and for the isotropic or cubic case with only one length scale parameter ℓ, it reduces to

$$G^{\Delta L}(\boldsymbol{x}) = \frac{1}{2\pi}\left(\ln r + K_0\left(r/\ell\right)\right). \tag{64}$$

Dislocation key-equations

In this section, we derive expressions for dislocation key-equations of straight dislocation from the general 3D dislocation key-equations.

General case

In the non-singular theory of dislocations, which is based on simplified anisotropic strain gradient elasticity, the 3D dislocation key-equations read (Po et al. 2018; Lazar and Po 2018a)

- *anisotropic Mura-Willis-like equation* for the non-singular elastic distortion tensor

$$\beta_{ik} = \epsilon_{knr}\mathbb{C}_{jmln}\partial_m G_{ij} * \alpha^0_{lr} \tag{65}$$

- *anisotropic Burgers-like equation* for the non-singular displacement vector

$$u_i = \partial_k G^{\Delta L} * \beta^{\mathrm{P},0}_{ik} - \epsilon_{knr}\mathbb{C}_{jklm}F_{mnij} * \alpha^0_{lr} \tag{66}$$

- *anisotropic Blin's-like formula* for the elastic interaction energy

$$W_{(AB)} = \int_{\mathbb{R}^3} \epsilon_{qns}\mathbb{C}_{psit}\epsilon_{tkr}\mathbb{C}_{jmlk}\left(F_{mnij} * \alpha^{0(A)}_{lr}\right)\alpha^{0(B)}_{pq}\,\mathrm{d}V \tag{67}$$

- *anisotropic Peach-Koehler-like stress equation* for the Cauchy stress tensor

$$\sigma_{pq} = \mathbb{C}_{pqik}\epsilon_{knr}\mathbb{C}_{jmln}\partial_m G_{ij} * \alpha^0_{lr} \tag{68}$$

- *Peach-Koehler force* for a dislocation density in the stress field of another dislocation

$$\mathcal{F}_k^{\mathrm{PK}} = \int_{\mathbb{R}^3} \epsilon_{kji}\sigma_{lj}\alpha_{li}^0 \,\mathrm{d}V\,. \tag{69}$$

Moreover, the dislocation density tensor and the plastic dislocation tensor are given by

$$\alpha_{ij} = G^L * \alpha_{ij}^0 \tag{70}$$

and

$$\beta_{ij}^{\mathrm{P}} = G^L * \beta_{ij}^{\mathrm{P},0}\,, \tag{71}$$

where it can be seen that the Green function G^L plays the role as a dislocation spreading function (Lazar 2014).

Generalized plane strain of straight dislocations

Now, we consider straight dislocations with line direction parallel to the x_3-axis belonging to the framework of generalized plane strain which is 2D elasticity consisting of plane strain and anti-plane strain. In general, the plane strain and antiplane strain fields do not decouple due to the anisotropy. Only for an orthotropic system, the plane strain and antiplane strain fields are separable. In generalized plane strain, all dislocation fields are independent of the variable x_3, all derivatives with respect to the x_3-axis vanish, $\partial_3 = 0$ and $\boldsymbol{x} \in \mathbb{R}^2$. Therefore, all dislocation fields depend only on x_1 and x_2 and are two-dimensional fields.

For generalized plane strain of dislocations, Eqs. (70) and (71) become

$$\alpha_{i3} = G^L * \alpha_{i3}^0\,, \qquad i = 1,2,3 \tag{72}$$

and

$$\beta_{i2}^{\mathrm{P}} = G^L * \beta_{i2}^{\mathrm{P},0}\,, \qquad i = 1,2,3\,. \tag{73}$$

For generalized plane strain of dislocations, the 2D dislocation-key Eqs. (65)–(69) reduce to

- *anisotropic Mura-Willis-like equation* for the non-singular elastic distortion tensor

$$\beta_{ik} = \epsilon_{kn3}\mathbb{C}_{jmln}\partial_m G_{ij} * \alpha_{l3}^0\,, \qquad i,j,l = 1,2,3 \qquad k,m,n = 1,2 \tag{74}$$

- *anisotropic Burgers-like equation* for the non-singular displacement vector

$$u_i = \partial_2 G^{\Delta L} * \beta_{i2}^{\mathrm{P},0} - \epsilon_{kn3}\mathbb{C}_{jklm}F_{mnij} * \alpha_{l3}^0 \tag{75}$$

with $i,j,l = 1,2,3$ and $k,m,n = 1,2$

- *anisotropic Blin's-like formula* for the elastic strain energy

$$W_{(AB)} = \int_{\mathbb{R}^3} \epsilon_{3ns}\mathbb{C}_{psit}\epsilon_{tk3}\mathbb{C}_{jmlk}\left(F_{mnij} * \alpha_{l3}^{0(A)}\right)\alpha_{p3}^{0(B)}\,\mathrm{d}V \tag{76}$$

with $i,j,l,p = 1,2,3$ and $k,m,n,s,t = 1,2$

- *anisotropic Peach-Koehler-like stress equation* equation for the Cauchy stress tensor

$$\sigma_{pq} = \mathbb{C}_{pqik}\epsilon_{kn3}\mathbb{C}_{jmln}\partial_m G_{ij} * \alpha^0_{l3} \tag{77}$$

- *Peach-Koehler force*

$$\mathcal{F}^{\mathrm{PK}}_k = \int_{\mathbb{R}^3} \epsilon_{kj3}\sigma_{lj}\alpha^0_{l3}\,\mathrm{d}V\,. \tag{78}$$

Dislocation key-equations of straight dislocations

Now, we consider straight dislocations with line direction parallel to the x_3-axis and defect surface in the x_1x_3 half plane for negative x_1 ($x_2 = 0$, $x_1 < 0$). For a straight dislocation with Burgers vector b_i located at $(x_1, x_2) = (0,0)$, the classical dislocation density and the classical plastic distortion are given by (see also deWit (1973b); Mura (1987))

$$\alpha^0_{i3} = b_i\,\delta(x_1)\delta(x_2) \tag{79}$$

and

$$\beta^{\mathrm{P},0}_{i2} = b_i\,\delta(x_2)H(-x_1) = b_i\,\delta(x_2)\int_{x_1}^{\infty}\delta(X)\,\mathrm{d}X\,, \tag{80}$$

which possesses a discontinuity at $x_2 = 0$ for $x_1 < 0$. Here $H(.)$ denotes the Heaviside step function.

If we substitute Eqs. (79) and (80) into Eqs. (72) and (73), respectively, we obtain for the dislocation density of a straight dislocation

$$\alpha_{i3} = \frac{b_i}{2\pi}\frac{1}{\sqrt{\det\boldsymbol{\Lambda}}}K_0\Big(\sqrt{\boldsymbol{x}^T(\boldsymbol{\Lambda}^{-1})\boldsymbol{x}}\Big) \tag{81}$$

and for the plastic distortion of a straight dislocation

$$\beta^{\mathrm{P}}_{i2} = \frac{b_i}{2\pi}\frac{1}{\sqrt{\det\boldsymbol{\Lambda}}}\int_{x_1}^{\infty}K_0\Big(\sqrt{\boldsymbol{x}'^T(\boldsymbol{\Lambda}^{-1})\boldsymbol{x}'}\Big)\mathrm{d}X\,, \tag{82}$$

where $\boldsymbol{x}' = (X, x_2)$. In general, the dislocation density tensor defines the dislocation core region and determines the shape and size of the dislocation core (see also Hartley and Mishin (2005); Lazar (2013, 2017)). For that reason, one can call α_{ij} the dislocation core tensor. The dislocation density (81) is only non-zero in the dislocation core. Equation (81) models the dislocation core in the x_1x_2-plane with anisotropic shape (core anisotropy) depending on the 3 length scale parameters Λ_{11}, Λ_{22} and Λ_{12}. The dislocation density (81) gives with 3 length scale parameters Λ_{11}, Λ_{22} and Λ_{12} a rotated elliptical dislocation core shape (see Fig. 3) and with 2 length scale parameters Λ_{11} and Λ_{22} an elliptical dislocation core shape (see Fig. 4). For $\Lambda_{11} = \Lambda_{22}$ and $\Lambda_{12} = 0$, the dislocation core has a circular shape (see below).

Substituting Eq. (79) into Eq. (74), the non-singular elastic distortion tensor of a straight dislocation in an infinite anisotropic medium reads as

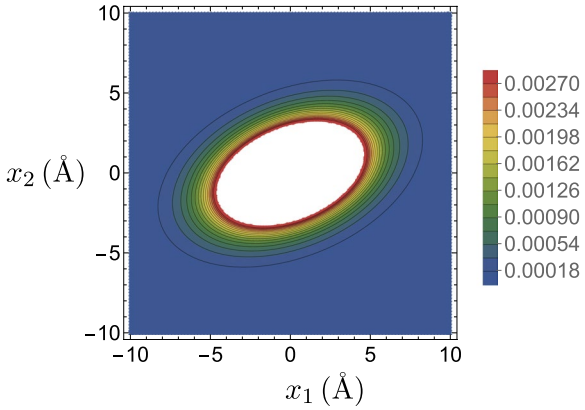

Fig. 3 Contour plot of the dislocation density $\boldsymbol{\alpha}_{i3}$ of a straight dislocation (normalized by the Burgers vector b_i) for $\Lambda_{11} = 2\,\text{Å}^2$, $\Lambda_{22} = 1\text{Å}^2$ and $\Lambda_{12} = 1/2\,\text{Å}^2$

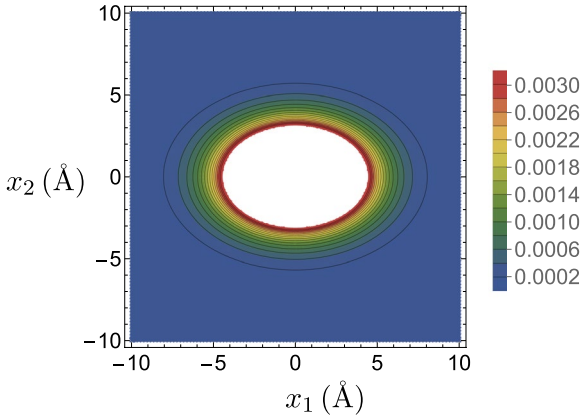

Fig. 4 Contour plot of the dislocation density $\boldsymbol{\alpha}_{i3}$ of a straight dislocation (normalized by the Burgers vector b_i) for $\Lambda_{11} = 2\,\text{Å}^2$, $\Lambda_{22} = 1\text{Å}^2$ and $\Lambda_{12} = 0$

$$\beta_{ik}(\boldsymbol{x}) = b_l \epsilon_{kn3} \mathbb{C}_{lnjm} \partial_m G_{ij}(\boldsymbol{x}) \tag{83}$$

and explicitly it becomes using Eq. (51)

$$\begin{aligned}\beta_{ik}(\boldsymbol{x}) = -\frac{b_l}{4\pi^2}\,\epsilon_{kn3}\mathbb{C}_{lnjm} \int_0^{2\pi} \hat{L}_{ij}^{-1}(\boldsymbol{\kappa})\,\frac{\kappa_m}{\boldsymbol{\kappa}\cdot\boldsymbol{x}} \\ \times \left[1 - \frac{\sqrt{\pi}\,(\boldsymbol{\kappa}\cdot\boldsymbol{x})^2}{4\lambda^2(\boldsymbol{\kappa})}\, G^{2,1}_{1,3}\left(\frac{(\boldsymbol{\kappa}\cdot\boldsymbol{x})^2}{4\lambda^2(\boldsymbol{\kappa})}\,\middle|\, \begin{matrix} -1 \\ -1,\ 0,\ -\frac{1}{2}\end{matrix}\right)\right] \mathrm{d}\phi\,.\end{aligned} \tag{84}$$

Equation (84) represents the gradient-extension of the Barnett-Swanger (Barnett and Swanger 1971) formula for the elastic distortion of a straight dislocation in classical anisotropic elasticity. In Eq. (84), $\hat{L}_{ij}^{-1}(\boldsymbol{\kappa})$ describes the bulk anisotropy and $\lambda^2(\boldsymbol{\kappa})$ describes the core anisotropy.

Using Eq. (79), the Cauchy stress tensor of a straight dislocation (77) becomes

$$\sigma_{pq}(\boldsymbol{x}) = b_l \mathbb{C}_{pqik} \epsilon_{kn3} \mathbb{C}_{lnjm} \partial_m G_{ij}(\boldsymbol{x})\,. \tag{85}$$

Using Eq. (51), it reads as

$$\sigma_{pq}(\boldsymbol{x}) = -\frac{b_l}{4\pi^2}\,\mathbb{C}_{pqik}\epsilon_{kn3}\mathbb{C}_{lnjm}\int_0^{2\pi}\hat{L}_{ij}^{-1}(\boldsymbol{\kappa})\,\frac{\kappa_m}{\boldsymbol{\kappa}\cdot\boldsymbol{x}} \times\left[1-\frac{\sqrt{\pi}\,(\boldsymbol{\kappa}\cdot\boldsymbol{x})^2}{4\lambda^2(\boldsymbol{\kappa})}\,G^{2,1}_{1,3}\left(\frac{(\boldsymbol{\kappa}\cdot\boldsymbol{x})^2}{4\lambda^2(\boldsymbol{\kappa})}\,\middle|\,\begin{matrix}-1\\-1,\ 0,\ -\frac{1}{2}\end{matrix}\right)\right]\mathrm{d}\phi\,. \tag{86}$$

Using Eqs. (79) and (80), the displacement vector of a straight dislocation (75) reduces to

$$u_i(\boldsymbol{x}) = \frac{b_i}{2\pi}\Bigg(\arctan\frac{x_2}{x_1}+\pi H(-x_1)\,\mathrm{sgn}(x_2) +\frac{\sqrt{\pi}}{4\pi}\,\partial_2\int_{x_1}^{\infty}\int_0^{2\pi}G^{2,1}_{1,3}\left(\frac{(\boldsymbol{\kappa}\cdot\boldsymbol{x}')^2}{4\lambda^2(\boldsymbol{\kappa})}\,\middle|\,\begin{matrix}0\\0,\ 0,\ \frac{1}{2}\end{matrix}\right)\mathrm{d}\phi\,\mathrm{d}X\Bigg) - b_l\epsilon_{kn3}\mathbb{C}_{jklm}F_{mnij}(\boldsymbol{x})\,, \tag{87}$$

where the $\boldsymbol{F}$-tensor is given in Eq. (59). Eq. (87) is the gradient-extension of the displacement field of a straight dislocation in classical anisotropic elasticity (see Lazar (2021)).

Using Eq. (79), the elastic interaction energy per unit length of two straight dislocations with Burgers vectors $b_l^{(A)}$ and $b_p^{(B)}$ reads

$$W_{(AB)} = b_l^{(A)}b_p^{(B)}\epsilon_{3ns}\mathbb{C}_{psit}\epsilon_{tk3}\mathbb{C}_{jmlk}F_{mnij}(\boldsymbol{x}^{(A)}-\boldsymbol{x}^{(B)})\,. \tag{88}$$

If we use Eq. (79), the Peach-Koehler force per unit length of a straight dislocation with Burgers vector b_l in a stress field σ_{jl} reads as

$$\mathcal{F}_k^{\mathrm{PK}} = \epsilon_{kj3}\sigma_{jl}b_l\,. \tag{89}$$

Straight dislocations in cubic materials

Let us consider straight dislocations in cubic materials. For cubic symmetry, $\Lambda_{11}=\Lambda_{22}=\ell^2$ and $\Lambda_{12}=0$, the dislocation density (81) and the plastic distortion (82) simplify to

$$\alpha_{i3} = \frac{b_i}{2\pi}\,\frac{1}{\ell^2}\,K_0\left(\frac{\sqrt{x_1^2+x_2^2}}{\ell}\right), \tag{90}$$

$$\beta^{\mathrm{p}}_{i2} = \frac{b_i}{2\pi}\,\frac{1}{\ell^2}\int_{x_1}^{\infty}K_0\left(\frac{\sqrt{X^2+x_2^2}}{\ell}\right)\mathrm{d}X\,. \tag{91}$$

The dislocation density (90) is plotted in Fig. 5 and gives the shape and size of the dislocation core of a straight dislocation in cubic crystals. Due to only one length scale parameter ℓ the dislocation core possesses a circular shape. Such a shape of the dislocation core of straight dislocations in cubic crystals is in good agreement with experimental results (see, e.g., Kret et al. (2000); Hartley and Mishin (2005)). The plastic distortion (91) is non-singular, smooth and finite as it can be seen in Fig. 6.

The elastic distortion tensor (84) and the Cauchy stress tensor (86) reduce to

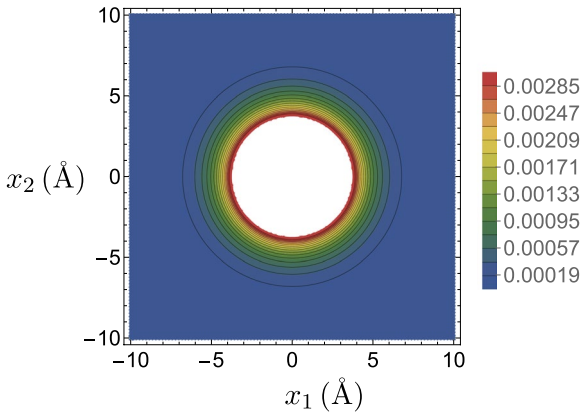

Fig. 5 Contour plot of the dislocation density $\boldsymbol{\alpha}_{i3}$ of a straight dislocation (normalized by the Burgers vector b_i) for fcc Al: $\ell = 1.1774$ Å

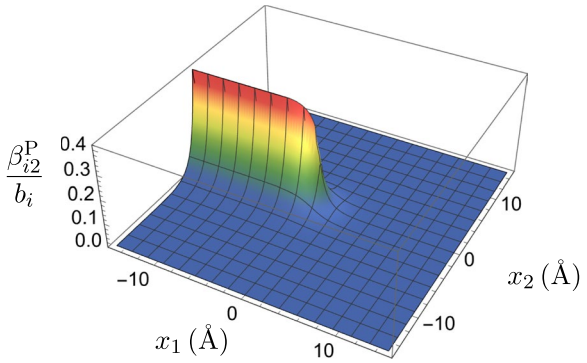

Fig. 6 Plastic distortion β^{P}_{i2} of a straight dislocation near the dislocation line for fcc Al: $\ell = 1.1774$ Å

$$\begin{aligned}\beta_{ik}(\boldsymbol{x}) = -\frac{b_l}{4\pi^2}\,\epsilon_{kn3}\mathbb{C}_{lnjm}\int_0^{2\pi}\hat{L}^{-1}_{ij}(\boldsymbol{\kappa})\,\frac{\kappa_m}{\boldsymbol{\kappa}\cdot\boldsymbol{x}}\\ \times\left[1-\frac{\sqrt{\pi}\,(\boldsymbol{\kappa}\cdot\boldsymbol{x})^2}{4\ell^2}\,G^{2,1}_{1,3}\left(\frac{(\boldsymbol{\kappa}\cdot\boldsymbol{x})^2}{4\ell^2}\,\middle|\,\begin{matrix}-1\\-1,\ 0,\ -\frac{1}{2}\end{matrix}\right)\right]\mathrm{d}\phi\end{aligned} \tag{92}$$

and

$$\begin{aligned}\sigma_{pq}(\boldsymbol{x}) = -\frac{b_l}{4\pi^2}\,\mathbb{C}_{pqik}\epsilon_{kn3}\mathbb{C}_{lnjm}\int_0^{2\pi}\hat{L}^{-1}_{ij}(\boldsymbol{\kappa})\,\frac{\kappa_m}{\boldsymbol{\kappa}\cdot\boldsymbol{x}}\\ \times\left[1-\frac{\sqrt{\pi}\,(\boldsymbol{\kappa}\cdot\boldsymbol{x})^2}{4\ell^2}\,G^{2,1}_{1,3}\left(\frac{(\boldsymbol{\kappa}\cdot\boldsymbol{x})^2}{4\ell^2}\,\middle|\,\begin{matrix}-1\\-1,\ 0,\ -\frac{1}{2}\end{matrix}\right)\right]\mathrm{d}\phi\,,\end{aligned} \tag{93}$$

respectively.

The displacement vector (87) becomes

$$\begin{aligned} u_i(\boldsymbol{x}) = \frac{b_i}{2\pi}\Bigg(& \arctan\frac{x_2}{x_1} + \pi H(-x_1)\,\mathrm{sgn}(x_2) \\ & - x_2\int_{x_1}^{\infty} \frac{1}{\ell\sqrt{X^2+x_2^2}}\,K_1\left(\frac{\sqrt{X^2+x_2^2}}{\ell}\right)\mathrm{d}X\Bigg) \\ & + \frac{b_l}{4\pi^2}\,\epsilon_{kn3}\mathbb{C}_{jklm}\int_0^{2\pi}\hat{L}_{ij}^{-1}(\boldsymbol{\kappa})\,\kappa_m\kappa_n\Bigg[\gamma + \ln|\boldsymbol{\kappa}\cdot\boldsymbol{x}| \\ & + \frac{\sqrt{\pi}}{2}\,G_{1,3}^{2,1}\left(\frac{(\boldsymbol{\kappa}\cdot\boldsymbol{x})^2}{4\ell^2}\,\middle|\,\begin{matrix}0\\0,\ 0,\ \frac{1}{2}\end{matrix}\right)\Bigg]\mathrm{d}\phi\,. \end{aligned} \tag{94}$$

Simplified anisotropic strain gradient elasticity provides a regularization of the classical singular dislocation fields for cubic crystals with one regularization parameter ℓ in terms of Meijer G-functions and modified Bessel functions leading to a non-singular near-field in the dislocation core.

Material parameters for cubic crystals

In Mindlin's first strain gradient elasticity theory, the elastic constants and the gradient-elastic constants are characteristic material parameters which can be computed from interatomic potentials (see, e.g., Admal et al. (2017); Po et al. (2019)) or via ab initio DFT calculations (see, e.g., Shodja et al. (2018)). For some important cubic materials such as Al, Cu, Fe and W, the 3 elastic constants and 11 gradient-elastic constants have been computed using a second nearest-neighbour modified embedded-atom-method (2NN MEAM) interatomic potential (Admal et al. 2017; Po et al. 2019; Lazar et al. 2022).

We consider a cubic crystal with centrosymmetry. Let the Cartesian coordinate axes x_1, x_2 and x_3 coincide with the cubic crystal directions [100], [010] and [001], respectively. For cubic crystals, the fourth-rank constitutive tensor $\mathbb{C}_{ijkl}$, which is the tensor of elastic constants, is given by (see, e.g., Dederichs and Leibfried (1969); Bacon et al. (1980); Lazar et al. (2022))

$$\mathbb{C}_{ijkl} = C_{12}\,\delta_{ij}\delta_{kl} + C_{44}\big(\delta_{ik}\delta_{jl}+\delta_{il}\delta_{jk}\big) + (C_{11}-C_{12}-2C_{44})\,\delta_{ijkl} \tag{95}$$

with

$$\delta_{ijkl} = \sum_{s=1}^{3} e_i^{(s)}e_j^{(s)}e_k^{(s)}e_l^{(s)}\,, \tag{96}$$

where $\boldsymbol{e}^{(1)}$, $\boldsymbol{e}^{(2)}$, $\boldsymbol{e}^{(3)}$ are the (orthogonal) unit vectors of the cubic system. Because the coordinate system coincide with the cubic system, it yields $\delta_{ijkl}=1$ if $i=j=k=l$ and $\delta_{ijkl}=0$ otherwise (Dederichs and Leibfried 1969). In Eq. (95), C_{11}, C_{12} and C_{44} are the 3 independent elastic constants of a cubic crystal.

The inverse elastic tensor $\mathbb{C}^{-1}_{ijkl}$, which is the tensor of elastic compliances $\mathbb{S}_{ijkl}\equiv\mathbb{C}^{-1}_{ijkl}$, reads as

$$\mathbb{S}_{ijkl} = S_{12}\,\delta_{ij}\delta_{kl} + S_{44}\big(\delta_{ik}\delta_{jl} + \delta_{il}\delta_{jk}\big) + (S_{11} - S_{12} - 2S_{44})\,\delta_{ijkl} \tag{97}$$

with (see Hirth and Lothe (1982); Wooster (1978))

$$S_{11} = \frac{C_{11} + C_{12}}{(C_{11} - C_{12})(C_{11} + 2C_{12})} \tag{98}$$

$$S_{12} = -\frac{C_{12}}{(C_{11} - C_{12})(C_{11} + 2C_{12})} \tag{99}$$

$$S_{44} = \frac{1}{4C_{44}}\,. \tag{100}$$

This tensor is defined by the property (Teodosiu 1982)

$$\mathbb{C}_{ijmn}\mathbb{S}_{mnkl} = \frac{1}{2}\big(\delta_{ik}\delta_{jl} + \delta_{il}\delta_{jk}\big) \tag{101}$$

and therefore

$$\mathbb{C}_{ijkl}\mathbb{S}_{ijkl} = \mathbb{S}_{ijkl}\mathbb{C}_{ijkl} = 6\,. \tag{102}$$

For cubic crystals of point group $m\bar{3}m$ (cubic hexoctahedral), the sixth-rank constitutive tensor $\mathbb{D}_{ijmkln}$ in Mindlin's first strain gradient elasticity is given by (see, e.g., Lazar et al. (2022); Lazar and Agiasofitou (2023))

$$\begin{aligned}
\mathbb{D}_{ijmkln} = {} & \frac{a_1}{2}\big(\delta_{ij}\delta_{km}\delta_{ln} + \delta_{ij}\delta_{kn}\delta_{lm} + \delta_{kl}\delta_{im}\delta_{jn} + \delta_{kl}\delta_{in}\delta_{jm}\big) \\
& + 2a_2\,\delta_{ij}\delta_{kl}\delta_{mn} \\
& + \frac{a_3}{2}\big(\delta_{jk}\delta_{im}\delta_{ln} + \delta_{ik}\delta_{jm}\delta_{ln} + \delta_{il}\delta_{jm}\delta_{kn} + \delta_{jl}\delta_{im}\delta_{kn}\big) \\
& + a_4\big(\delta_{il}\delta_{jk}\delta_{mn} + \delta_{ik}\delta_{jl}\delta_{mn}\big) \\
& + \frac{a_5}{2}\big(\delta_{jk}\delta_{in}\delta_{lm} + \delta_{ik}\delta_{jn}\delta_{lm} + \delta_{jl}\delta_{km}\delta_{in} + \delta_{il}\delta_{km}\delta_{jn}\big) \\
& + a_6\big(\delta_{ik}\delta_{jlmn} + \delta_{il}\delta_{jkmn} + \delta_{jk}\delta_{ilmn} + \delta_{jl}\delta_{ikmn}\big) \\
& + a_7\big(\delta_{km}\delta_{ijln} + \delta_{lm}\delta_{ijkn} + \delta_{in}\delta_{jklm} + \delta_{jn}\delta_{iklm}\big) \\
& + a_8\,\delta_{mn}\delta_{ijkl} + a_9\big(\delta_{ij}\delta_{klmn} + \delta_{kl}\delta_{ijmn}\big) \\
& + a_{10}\big(\delta_{im}\delta_{jkln} + \delta_{jm}\delta_{ikln} + \delta_{kn}\delta_{ijlm} + \delta_{ln}\delta_{ijkm}\big) \\
& + a_{11}\,\delta_{ijklmn}
\end{aligned} \tag{103}$$

with

$$\delta_{ijklmn} = \sum_{s=1}^{3} e_i^{(s)} e_j^{(s)} e_k^{(s)} e_l^{(s)} e_m^{(s)} e_n^{(s)}\,. \tag{104}$$

Here, $a_1, \ldots, a_{11}$ are the 11 gradient-elastic constants of a cubic crystal with centrosymmetry and $\delta_{ijklmn} = 1$ if $i = j = k = l = m = n$ and $\delta_{ijklmn} = 0$ otherwise.

Table 1 Elastic and gradient-elastic constants computed from a second nearest-neighbor modified embedded-atom-method (2NN MEAM) interatomic potential for different cubic crystals (see Lazar et al. (2022))

	Al (fcc)	Cu (fcc)	Fe (bcc)	W (bcc)
C_{11} [eV/Å^3]	0.71366	1.09941	1.51659	3.32405
C_{12} [eV/Å^3]	0.38649	0.77973	0.86160	1.28028
C_{44} [eV/Å^3]	0.19704	0.51043	0.76096	1.01812
a_1 [eV/Å]	-0.02287	-0.08509	0.72859	1.43755
a_2 [eV/Å]	0.35854	0.23748	0.45980	0.87793
a_3 [eV/Å]	-0.24815	-0.03655	0.59810	0.19097
a_4 [eV/Å]	0.16786	0.03742	0.41599	0.85853
a_5 [eV/Å]	0.30012	0.07479	0.76600	1.23279
a_6 [eV/Å]	0.08229	0.23401	-0.58892	-0.67605
a_7 [eV/Å]	-0.13198	0.17426	-1.09107	-1.89998
a_8 [eV/Å]	-0.21058	0.18906	-1.08476	-2.30919
a_9 [eV/Å]	-0.54849	-0.02327	-1.32474	-3.33133
a_{10} [eV/Å]	0.41893	0.32059	-0.73389	-0.41688
a_{11} [eV/Å]	-0.19492	-2.86388	8.52704	14.79794

The tensor Λ_{mn} can also be estimated using the tensor $\mathbb{S}_{ijkl} = \mathbb{C}^{-1}_{ijkl}$. Multiplying both sides of Eq. (11) by $\mathbb{S}_{ijkl}$, we obtain $\mathbb{S}_{ijkl}\mathbb{D}_{ijmkln} = 6\Lambda_{mn}$, and therefore, the tensor Λ_{mn} can be given in terms of the two constitutive tensor $\mathbb{D}_{ijmkln}$ and $\mathbb{S}_{ijkl}$ as (Po et al. 2018)

$$\Lambda_{mn} = \frac{1}{6}\,\mathbb{S}_{ijkl}\mathbb{D}_{ijmkln}\,. \tag{105}$$

For cubic materials, the gradient length scale tensor Λ_{mn} reads (Po et al. 2018)

$$\Lambda_{mn} = \ell^2\delta_{mn}\,, \tag{106}$$

where ℓ is the characteristic length scale of simplified anisotropic strain gradient elasticity for cubic materials. The gradient length scale of cubic materials can be computed directly from the fourth-rank constitutive tensor $\mathbb{C}_{ijkl}$ and the sixth-rank constitutive tensor $\mathbb{D}_{ijmkln}$ using Eqs. (105) and (106) leading to the formula:

$$\ell^2 = \frac{1}{18}\,\mathbb{S}_{ijkl}\mathbb{D}_{ijmklm}\,. \tag{107}$$

If we substitute Eqs. (97) and (103) into Eq. (107), we obtain the following formula for the characteristic length in terms of the 3 elastic constants and the 11 gradient-elastic constants

$$\begin{aligned}\ell^2 = {}& \frac{3}{C_{44}}\,(a_3 + 3a_4 + a_5 + 2a_6) + \frac{6}{C_{11}+2C_{12}}\,(a_1 + 3a_2 + a_9)\\ &+ \frac{3(C_{11}+C_{12})}{(C_{11}+2C_{12})(C_{11}-C_{12})}(2a_3 + 6a_4 + 2a_5 + 4a_6 + 4a_7 + 3a_8 + 4a_{10} + a_{11}).\end{aligned} \tag{108}$$

Equation (108) gives an atomistic determination of the characteristic length ℓ from numeric values of the elastic and gradient-elastic constants computed from interatomic potentials or via ab initio DFT. Using the elastic and gradient-elastic constants of Al, Cu, Fe

Table 2 Characteristic length scale of simplified anisotropic strain gradient elasticity for different cubic crystals

	Al (fcc)	Cu (fcc)	Fe (bcc)	W (bcc)
ℓ [Å]	1.1774	0.7852	0.7420	0.8502
a [Å]	4.0495	3.6149	2.8665	3.1652
ℓ/a	0.2907	0.2172	0.2592	0.2688

Table 3 The anisotropy factor H given by Hirth and Lothe (1982) for the fourth-rank constitutive tensor $\mathbb{C}_{ijkl}$ for different cubic materials

	Al (fcc)	Cu (fcc)	Fe (bcc)	W (bcc)
$H = C_{11} - C_{12} - 2C_{44}$ [eV/Å^3]	0.06691	0.70118	0.86693	−0.00753

and W given in Table 1, the characteristic length ℓ of simplified anisotropic strain gradient elasticity is computed using Eq. (108) and reported in Table 2.

Elastic distortion and stress fields of screw and edge dislocations in cubic crystals

In order to illustrate the applicability of simplified anisotropic first strain gradient elasticity, we compute the elastic distortion and stress fields of both screw and edge dislocations in cubic crystals. The elastic distortion is computed according to the formula (92). The elastic distortion is dimensionless. The stress field is computed according to the stress formula (93). Stresses are in units of eV/Å^3. We choose bcc iron (Fe) and fcc copper (Cu) because they are crystals with high anisotropy of the elastic constants (see Table 3) and bcc tungsten (W) and fcc aluminum (Al) because they are crystals which are nearly isotropic with respect to the elastic constants (see Table 3). Therefore, the change of the dislocation fields from isotropic $\Longrightarrow$ anisotropic behaviour can be seen by comparing the dislocation fields for bcc: tungsten (W) $\Longrightarrow$ iron (Fe) and for fcc: aluminum (Al) $\Longrightarrow$ copper (Cu). We present the dislocation fields in contour plots in order to see the characteristic shape of the far- and near-fields of straight dislocations and the influence of the anisotropy of cubic crystals.

BCC Fe

In bcc Fe, we consider dislocations with Burgers vector $\boldsymbol{b} = a/2\,\langle 111\rangle$. The Burgers vector reads $b = \sqrt{3}/2\,a = 2.482$ Å. The elastic constants and the corresponding length of bcc Fe have been taken from Tables 1 and 2. Using these material constants, we compute the elastic distortion and stress fields in the plane orthogonal to infinite straight edge and screw $1/2[111](\bar{1}10)$ dislocations, which have line directions along the $[\bar{1}\bar{1}2]$ and [111] axes, respectively.

First, we give the plots of the non-singular elastic distortion components of a screw dislocation in bcc Fe using simplified anisotropic first strain gradient elasticity in Fig. 7. In Fig. 7, it can be seen that a screw dislocation in bcc Fe has pronounced elastic distortion components β_{zx} and β_{zy} (only these components are non-zero in the isotropic case); the other four components β_{xx}, β_{yy}, β_{xy} and β_{yx} are weak.

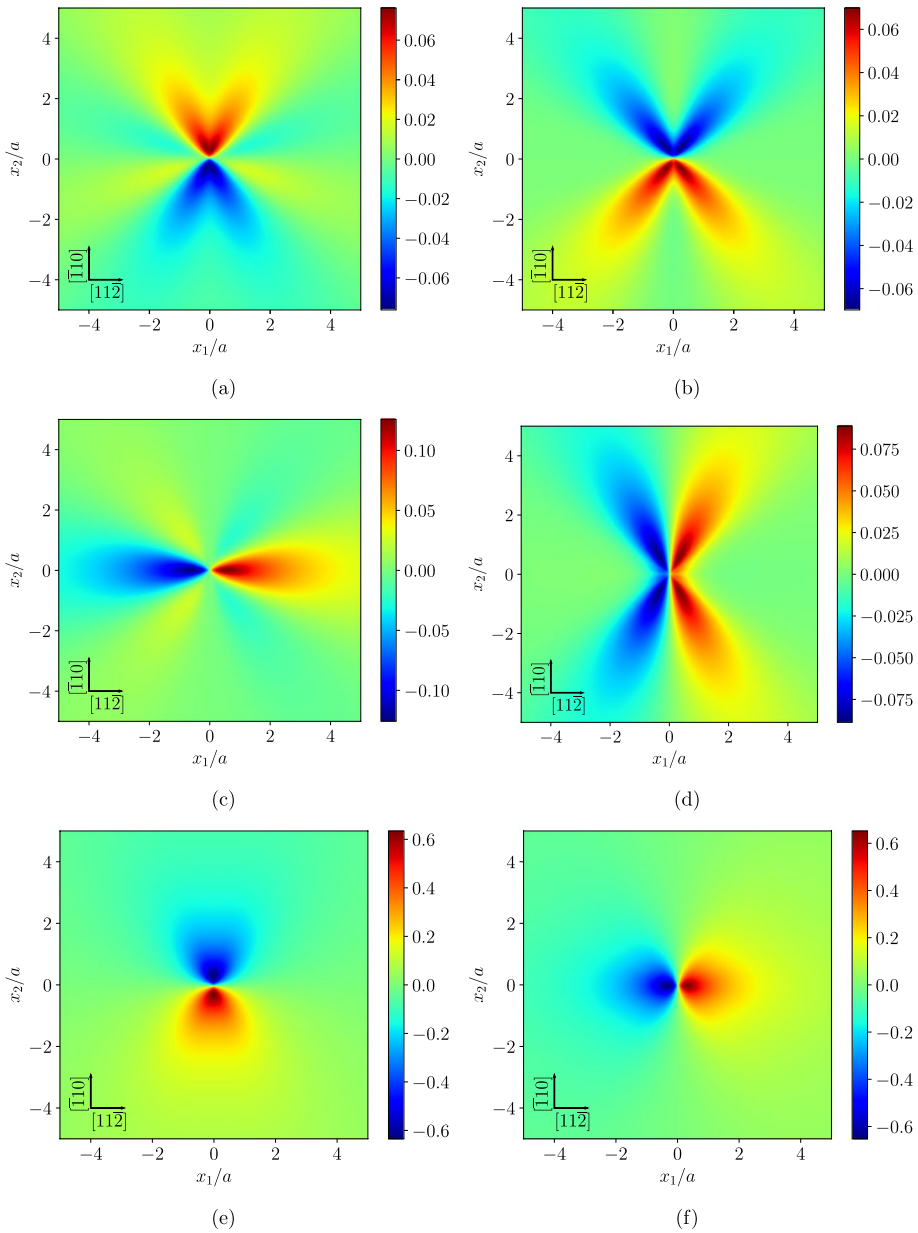

Fig. 7 Non-singular elastic distortion components of a screw dislocation in bcc Fe: **a** β_{xx}, **b** β_{yy}, **c** β_{xy}, **d** β_{yx}, **e** β_{zx}, **f** β_{zy}

The plots of the non-singular stress components of a screw dislocation in bcc Fe using simplified anisotropic first strain gradient elasticity are given in Fig. 8. It can be seen in Fig. 8 that a screw dislocation in bcc Fe possesses pronounced stress components σ_{xz} and σ_{yz} (only these components are non-zero in the isotropic case); the others are weak. The anisotropic stress components σ_{xz} and σ_{yz} (see Fig. 8e, f) do not differ greatly in form from the corresponding isotropic fields. In Fig. 8a–d, it is interesting to observe that in contrast to the isotropic case there are four additional but weaker stress components σ_{xx}, σ_{yy}, σ_{zz} and σ_{xy} (in comparison with the other two anisotropic components) in the anisotropic case reflecting the effects of anisotropy. In particular, in Fig. 8c, it can

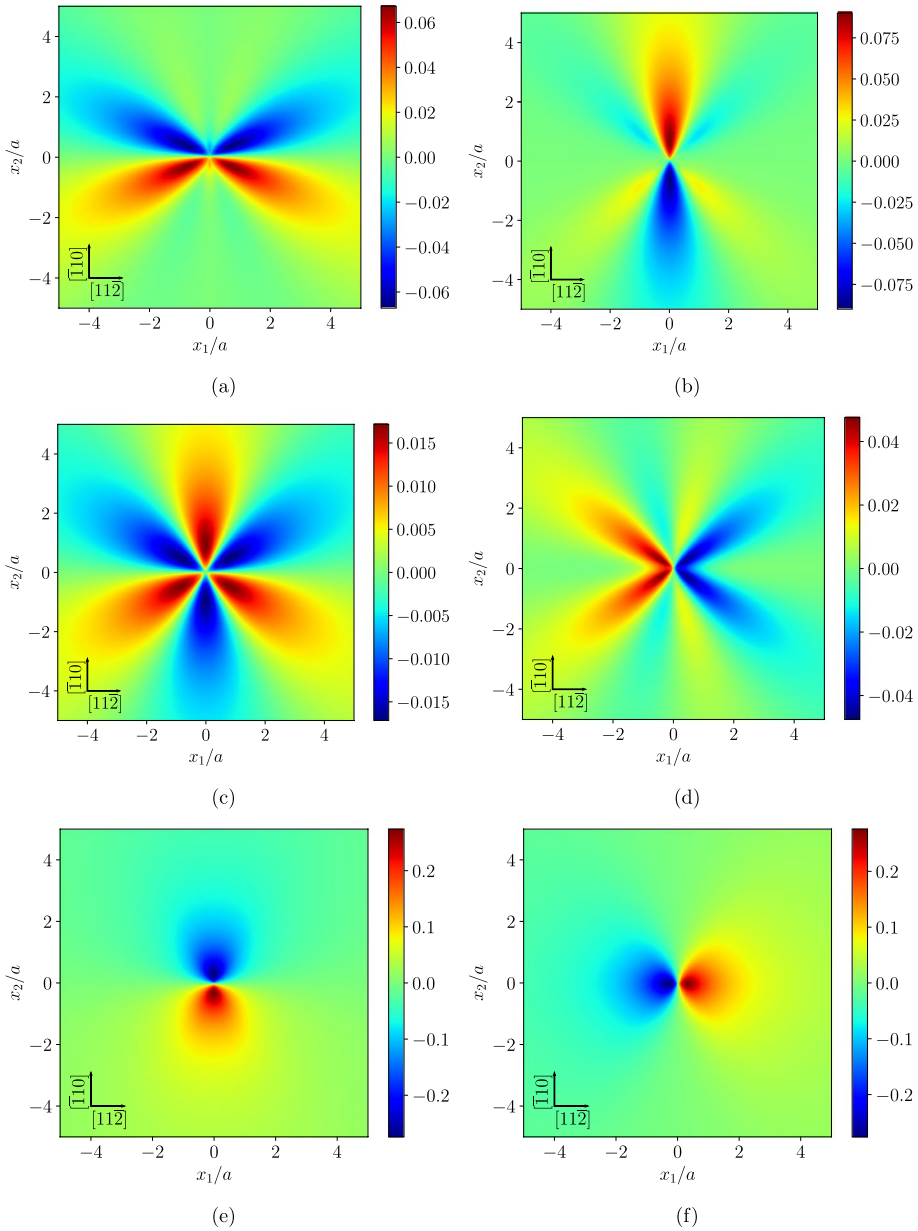

Fig. 8 Non-singular stress components of a screw dislocation in bcc Fe in units of eV/Å^3: **a** σ_{xx}, **b** σ_{yy}, **c** σ_{zz}, **d** σ_{xy}, **e** σ_{xz}, **f** σ_{yz}

be seen that the stress component σ_{zz} of a [111] screw dislocation in bcc Fe possesses a three-fold symmetry.

The plots of the six non-singular elastic distortion components of an edge dislocation in bcc Fe using simplified anisotropic first strain gradient elasticity are given in Fig. 9.

Next, we give the plots of the non-singular stress components of an edge dislocation in bcc Fe using simplified anisotropic first strain gradient elasticity in Fig. 10. It is seen from Fig. 10 that in the case of anisotropy the components of stress σ_{xz} and σ_{yz} of an edge dislocation are weak in comparison with the other four components σ_{xx}, σ_{yy}, σ_{zz} and σ_{xy}, but they are not zero as in the isotropic case. The anisotropic stress components

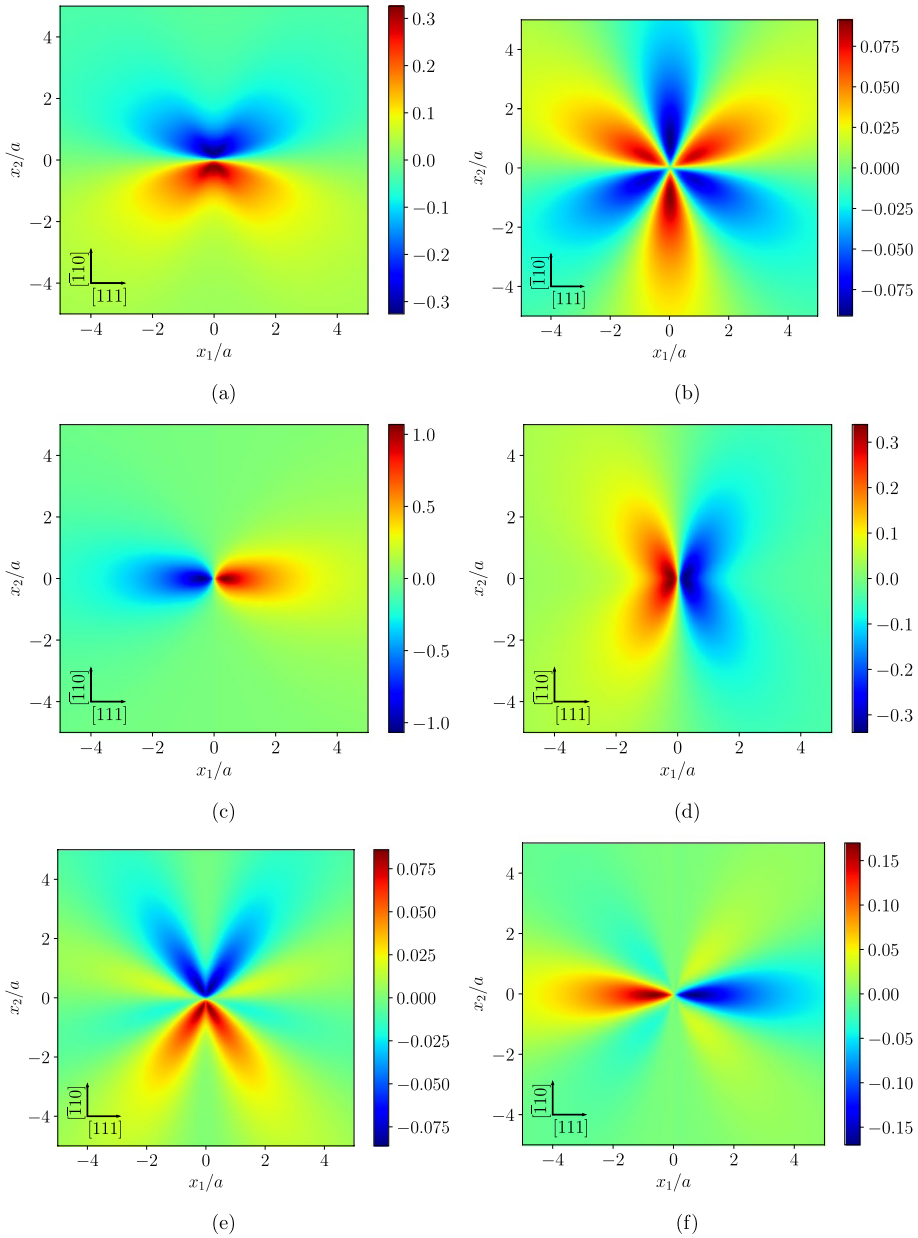

Fig. 9 Non-singular elastic distortion components of an edge dislocation in bcc Fe: **a** β_{xx}, **b** β_{yy}, **c** β_{xy}, **d** β_{yx}, **e** β_{zx}, **f** β_{zy}

σ_{xx}, σ_{yy} and σ_{xy} (see Fig. 10a, b and d) do not differ greatly in form from the corresponding isotropic fields which is not the case for the stress component σ_{zz} (see Fig. 10c). Due to the anisotropy, we have the appearance of two additional but weaker stress components (in comparison with the other anisotropic components), namely the σ_{xz} (Fig. 10e) and σ_{yz} (Fig. 10f).

As it can be seen in Figs. 7, 8, 9, and 10, the elastic distortion and stress fields of both screw and edge dislocations are non-singular. The symmetry of the (non-singular) elastic strain fields (symmetric part of the elastic distortion, see Eq. (2)) of a screw

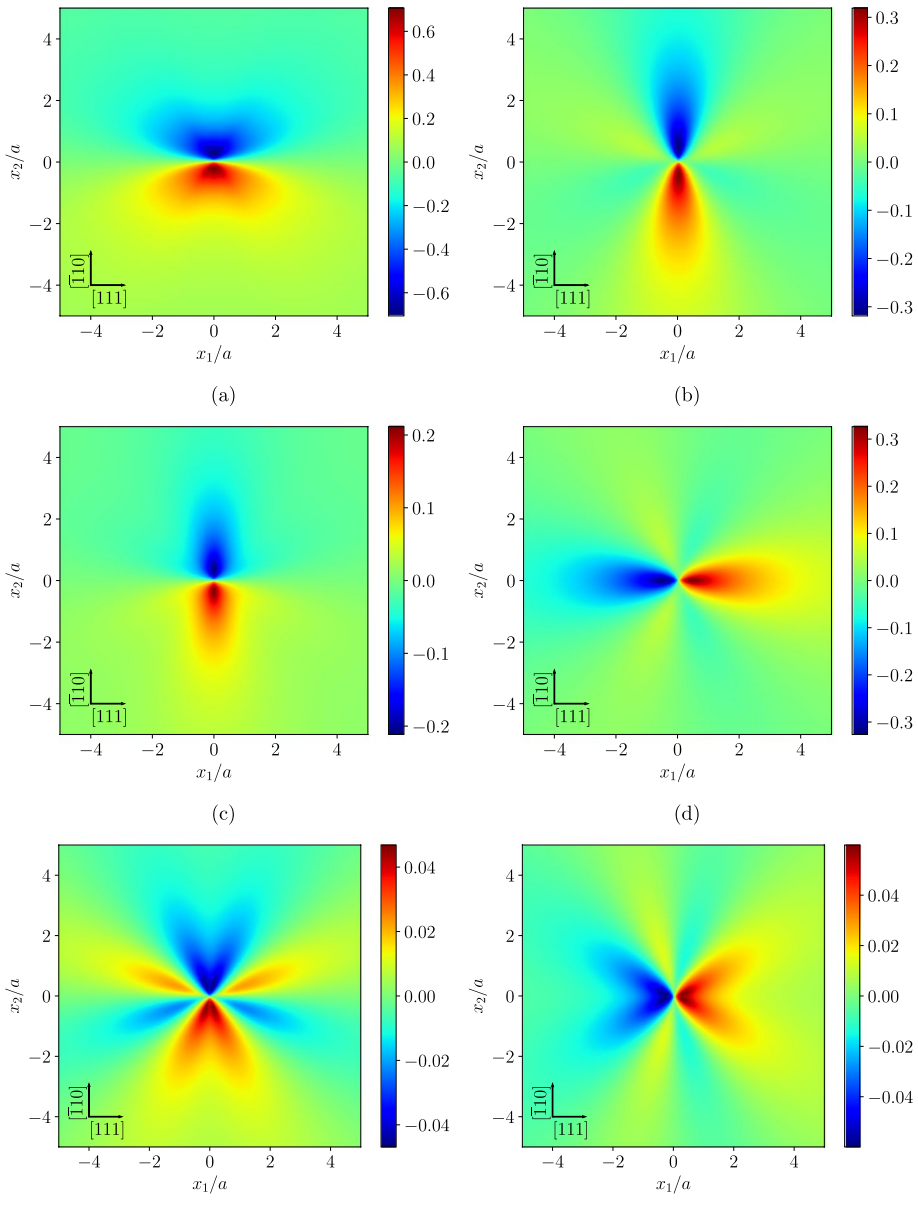

Fig. 10 Non-singular stress components of an edge dislocation in bcc Fe in units of eV/Å^3: **a** σ_{xx}, **b** σ_{yy}, **c** σ_{zz}, **d** σ_{xy}, **e** σ_{xz}, **f** σ_{yz}

dislocation (Fig. 7) and an edge dislocation (Fig. 9) using simplified anisotropic first strain gradient elasticity are in agreement with the symmetry of the (singular) elastic strain fields of a screw and an edge dislocation given in the framework of classical anisotropic elasticity by Yoo and Loh (1971). Moreover, the symmetry of the (non-singular) stress fields of a screw dislocation (Fig. 8) and an edge dislocation (Fig. 10) using simplified anisotropic first strain gradient elasticity agree with the symmetry of the (singular) stress fields of a screw and an edge dislocation given in the framework of classical anisotropic elasticity by Baštecká (1965) and Yoo and Loh (1971) (see also Steeds (1973)) and with the symmetry of the (non-singular) stress fields of a

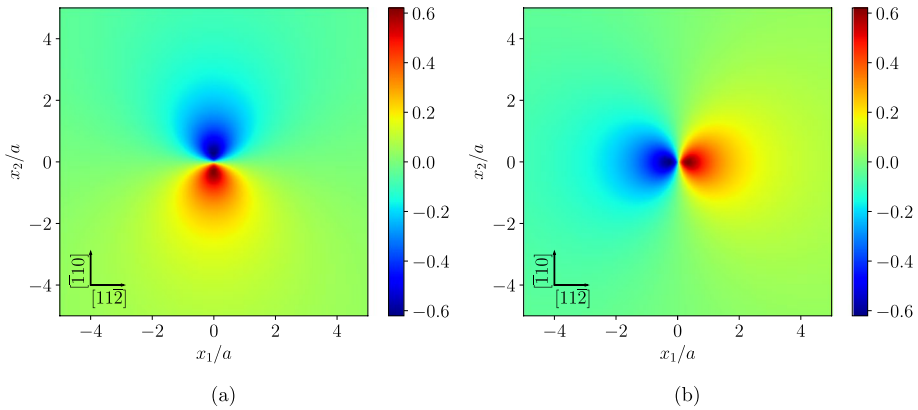

Fig. 11 Non-singular elastic distortion components of a screw dislocation in bcc W: **a** β_{zx}, **b** β_{zy}

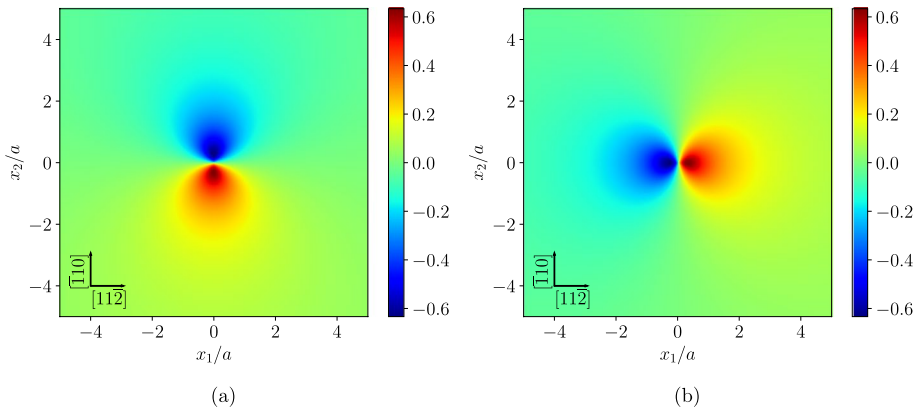

Fig. 12 Non-singular stress components of a screw dislocation in bcc W in units of eV/Å^3: **a** σ_{xz}, **b** σ_{yz}

screw and an edge dislocation given in the framework of nonlocal anisotropic elasticity by Lazar et al. (2020).

BCC W

In bcc W, we consider dislocations with Burgers vector $\boldsymbol{b} = a/2\,\langle 111\rangle$. The Burgers vector reads $b = \sqrt{3}/2\,a = 2.741$ Å. The elastic constants and the corresponding length of bcc W have been taken from Tables 1 and 2. Using these material constants, we compute the elastic distortion and stress fields in the plane orthogonal to infinite straight edge and screw $1/2[111](\bar{1}10)$ dislocations, which have line directions along the $[\bar{1}\bar{1}2]$ and [111] axes, respectively.

The plots of the non-singular elastic distortion components of a screw dislocation in bcc W using simplified anisotropic first strain gradient elasticity are given in Fig. 11. It can be seen that only the components β_{zx} and β_{zy} give a non-zero contribution since W is isotropic with respect to the elastic constants (see Table 3). The plots of the non-singular stress components of a screw dislocation in bcc W using simplified anisotropic first strain gradient elasticity are given in Fig. 12. It can be seen that only the components σ_{xz} and σ_{yz} give a non-zero contribution since W is isotropic with respect to the elastic constants (see Table 3).

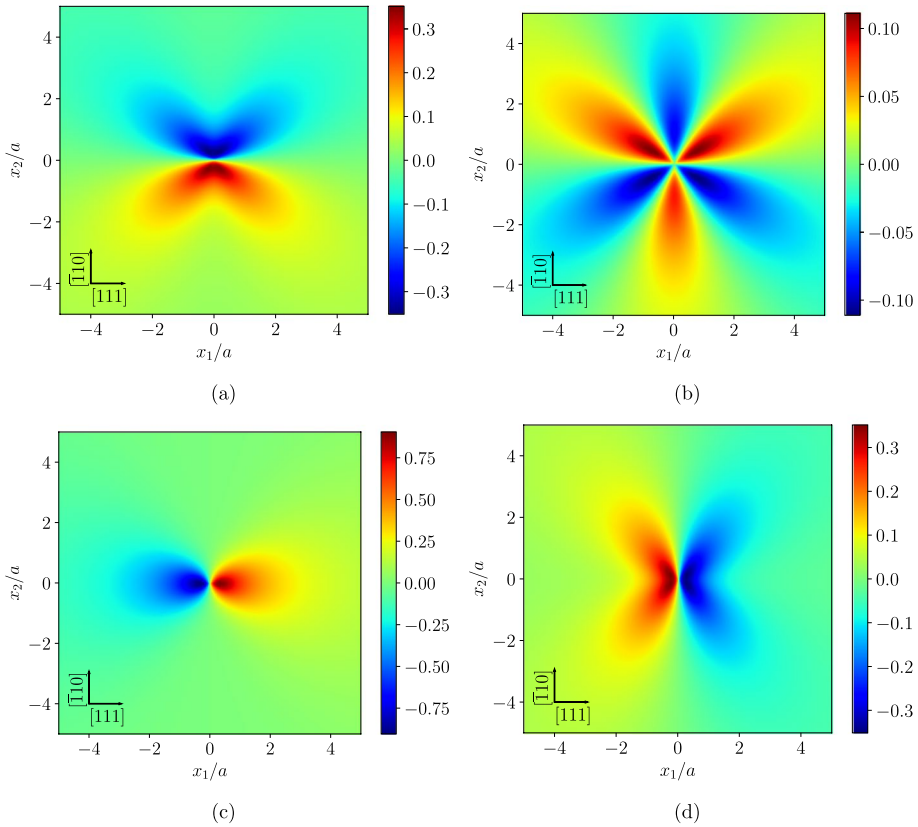

Fig. 13 Non-singular elastic distortion components of an edge dislocation in bcc W: **a** β_{xx}, **b** β_{yy}, **c** β_{xy}, **d** β_{yx}

The plots of the four non-singular elastic distortion components of an edge dislocation in bcc W using simplified anisotropic first strain gradient elasticity are given in Fig. 13. It can be seen from Fig. 13 that only the four components β_{xx}, β_{yy}, β_{xy} and β_{yx} give a non-zero contribution because W is isotropic. The plots of the non-singular stress components of an edge dislocation in bcc W using simplified anisotropic first strain gradient elasticity are given in Fig. 14. It can be seen from Fig. 14 that only the four components σ_{xx}, σ_{yy}, σ_{zz} and σ_{xy} give a non-zero contribution since W is isotropic. The shape of the plots of the stresses of an edge dislocation in W given in Fig. 14 agree with the plots given in Yoo and Loh (1970) (see also Steeds (1973)).

If we compare the dislocation fields of screw and edge dislocations in bcc iron in BCC Fe section and in bcc tungsten in BCC W section we observe some characteristic differences. On the one hand, bcc iron is strongly anisotropic and gives 6 nonzero dislocation fields for the elastic strain and the Cauchy stress tensors for both screw and edge dislocations. On the other hand, bcc tungsten is isotropic and gives 4 nonzero dislocation fields for the elastic strain and the Cauchy stress tensors of an edge dislocation and 2 nonzero dislocation fields for the elastic strain and the Cauchy stress tensors of a screw dislocation. The near-fields of the elastic strain and the Cauchy stress fields are non-singular due to the regularization and show a characteristic shape, namely they are zero at the dislocation line.

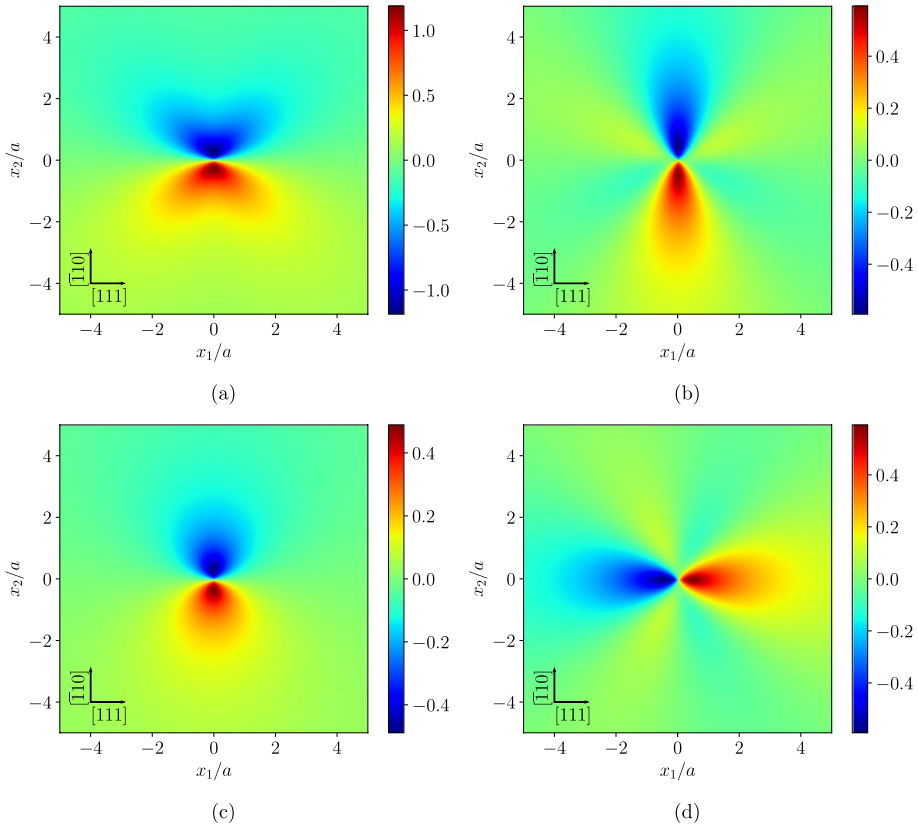

Fig. 14 Non-singular stress components of an edge dislocation in bcc W in units of eV/Å^3: **a** σ_{xx}, **b** σ_{yy}, **c** σ_{zz}, **d** σ_{xy}

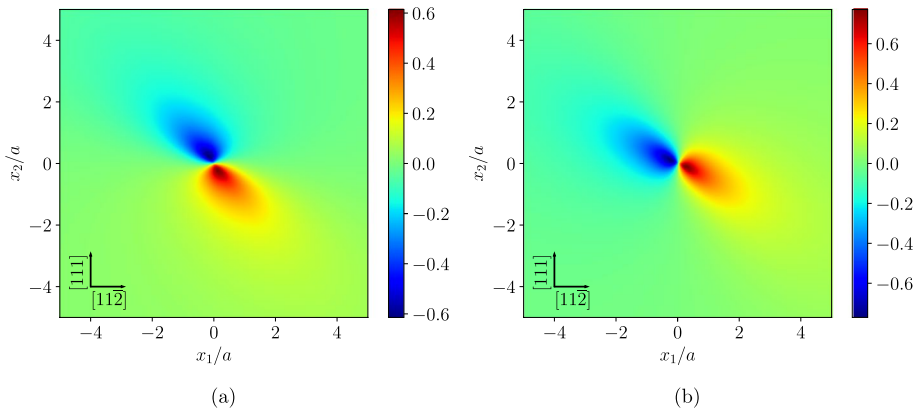

Fig. 15 Non-singular elastic distortion components of a screw dislocation in fcc Cu: **a** β_{zx}, **b** β_{zy}

FCC Cu

In fcc Cu, we consider dislocations with Burgers vector $\boldsymbol{b} = a/2\,\langle 110\rangle$. The Burgers vector reads $b = a/\sqrt{2} = 2.556\,\text{Å}$. The elastic constants and the corresponding length of fcc Cu have been taken from Tables 1 and 2. Using these material constants, we compute the elastic distortion and stress fields in the plane orthogonal to infinite

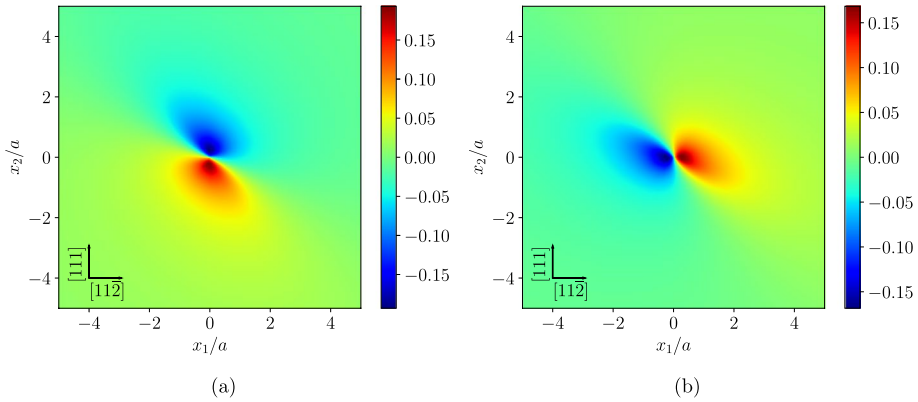

Fig. 16 Non-singular stress components of a screw dislocation in fcc Cu in units of eV/Å^3: **a** σ_{xz}, **b** σ_{yz}

straight edge and screw $1/2[1\bar{1}0](111)$ dislocations, which have line directions along the $[\bar{1}\bar{1}2]$ and $[1\bar{1}0]$ axes, respectively.

For a screw dislocation in fcc Cu, the plots of the two non-singular elastic distortion components are given in Fig. 15. The plots of the corresponding two non-singular stress components of a screw dislocation in fcc Cu using simplified anisotropic first strain gradient elasticity are given in Fig. 16. The shape and symmetry of the (non-singular) stress fields of a screw dislocation (Fig. 16) using simplified anisotropic first strain gradient elasticity agree with the symmetry of the (singular) stress fields of a screw dislocation given in the framework of classical anisotropic elasticity by Yoo and Loh (1970) (see also Steeds (1973)).

Using simplified anisotropic first strain gradient elasticity, the plots of the six non-singular elastic distortion components of an edge dislocation in fcc Cu are given in Fig. 17. The plots of the six non-singular stress components of an edge dislocation in fcc Cu using simplified anisotropic first strain gradient elasticity are given in Fig. 18. It is seen from Fig. 18 that in the case of anisotropy the components of stress σ_{xz} and σ_{yz} of an edge dislocation are weak in comparison with the other four components σ_{xx}, σ_{yy}, σ_{zz} and σ_{xy}, but they are not zero as in the isotropic case (see also Steeds (1973)). In particular, the component σ_{zz} shows a characteristic shape due to the elastic anisotropy.

As it can be seen in Figs. 15, 16, 17, and 18, the elastic distortion and stress fields of both screw and edge dislocations are non-singular.

FCC Al

In fcc Al, we consider dislocations with Burgers vector $\boldsymbol{b} = a/2\,\langle 110\rangle$. The Burgers vector reads $b = a/\sqrt{2} = 2.863$ Å. The elastic constants and the corresponding length of fcc Cu have been taken from Tables 1 and 2. Using these material constants, we compute the elastic distortion and stress fields in the plane orthogonal to infinite straight edge and screw $1/2[1\bar{1}0](111)$ dislocations, which have line directions along the $[\bar{1}\bar{1}2]$ and $[1\bar{1}0]$ axes, respectively.

The plots of the non-singular elastic distortion components of a screw dislocation in fcc Al using simplified anisotropic first strain gradient elasticity are given in Fig. 19. It can be seen that only the components β_{zx} and β_{zy} give a non-zero contribution since

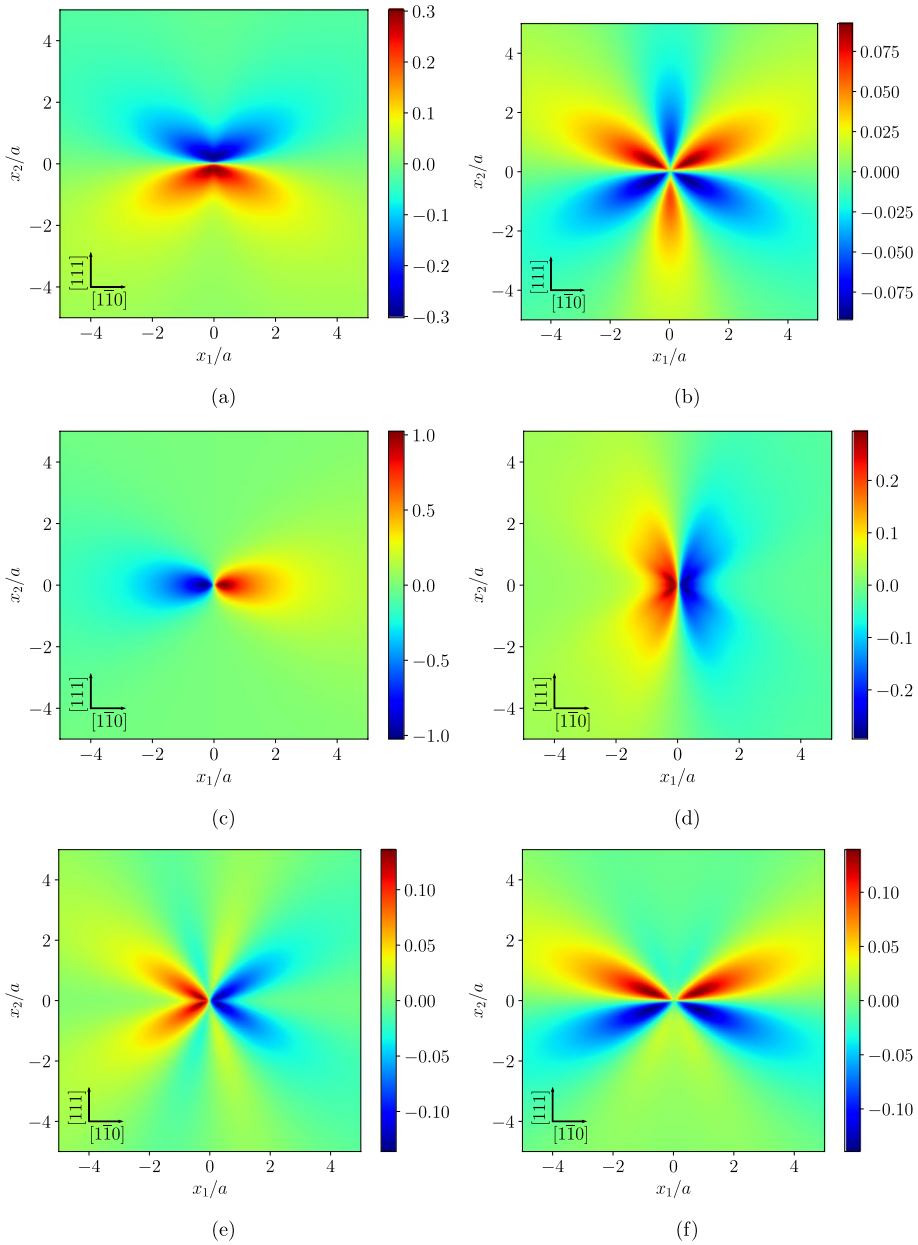

Fig. 17 Non-singular elastic distortion components of an edge dislocation in fcc Cu: **a** β_{xx}, **b** β_{yy}, **c** β_{xy}, **d** β_{yx}, **e** β_{zx}, **f** β_{zy}

Al is nearly isotropic with respect to the elastic constants (see Table 3). The plots of the non-singular stress components of a screw dislocation in fcc Al using simplified anisotropic first strain gradient elasticity are given in Fig. 20. It can be seen that only the components σ_{xz} and σ_{yz} give a non-zero contribution since Al is nearly isotropic with respect to the elastic constants (see Table 3). The shape of the plots of the stresses of a screw dislocation in Al given in Fig. 20 agree with the plots given in Yoo and Loh (1970) (see also Steeds (1973)).

The plots of the four non-singular elastic distortion components of an edge dislocation in fcc Al using simplified anisotropic first strain gradient elasticity are given in Fig. 21.

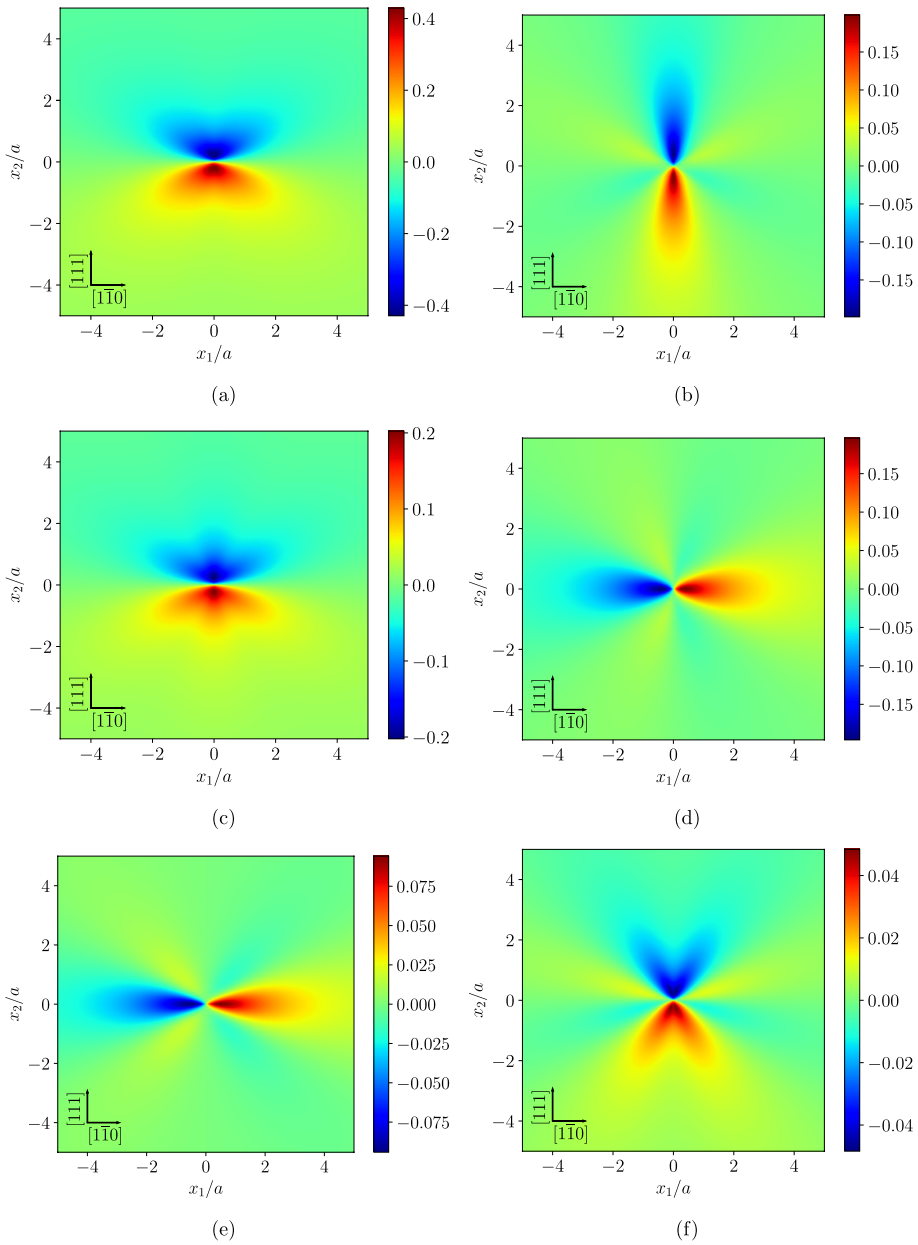

Fig. 18 Non-singular stress components of an edge dislocation in fcc Cu in units of eV/Å^3: **a** σ_{xx}, **b** σ_{yy}, **c** σ_{zz}, **d** σ_{xy}, **e** σ_{xz}, **f** σ_{yz}

It can be seen from Fig. 21 that only the four components β_{xx}, β_{yy}, β_{xy} and β_{yx} give a non-zero contribution because Al is nearly isotropic. The plots of the non-singular stress components of an edge dislocation in fcc Al using simplified anisotropic first strain gradient elasticity are given in Fig. 22. It can be seen from Fig. 22 that only the four components σ_{xx}, σ_{yy}, σ_{zz} and σ_{xy} give a non-zero contribution since Al is nearly isotropic.

If we compare the dislocation fields of screw and edge dislocations in fcc copper in FCC Cu section and in fcc aluminum in FCC Al section we observe some characteristic differences. On the one hand, fcc copper is strongly anisotropic and gives 6 nonzero

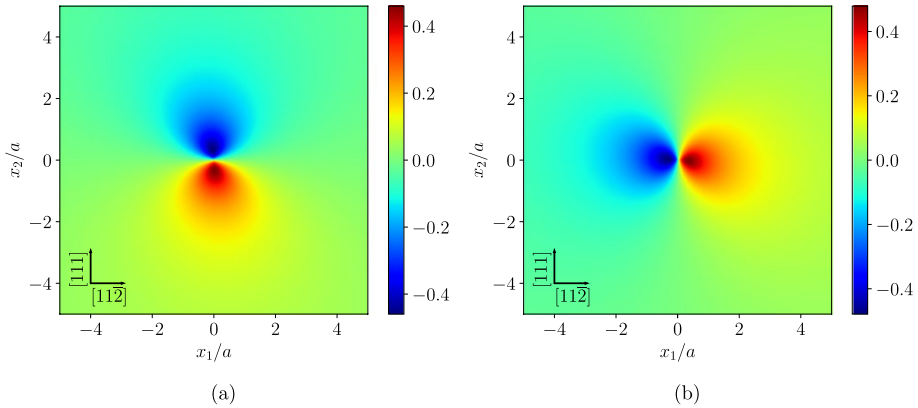

Fig. 19 Non-singular elastic distortion components of a screw dislocation in fcc Al: **a** β_{zx}, **b** β_{zy}

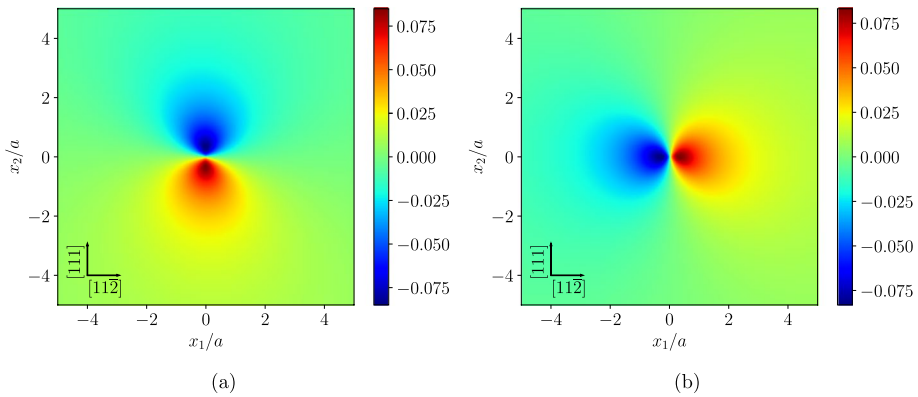

Fig. 20 Non-singular stress components of a screw dislocation in fcc Al in units of eV/Å^3: **a** σ_{xz}, **b** σ_{yz}

dislocation fields for the elastic strain and the Cauchy stress tensors for an edge dislocation and 2 nonzero dislocation fields for the elastic strain and the Cauchy stress tensors for a screw dislocation with a characteristic "rotated and deformed" shape. On the other hand, fcc aluminum is nearly isotropic and gives 4 nonzero dislocation fields for the elastic strain and the Cauchy stress tensors of an edge dislocation and 2 nonzero dislocation fields for the elastic strain and the Cauchy stress tensors of a screw dislocation. The near-fields of the elastic strain and the Cauchy stress fields are non-singular due to the regularization and show a characteristic shape, namely they are zero at the dislocation line.

Conclusions

In this work, we have presented a non-singular dislocation theory of straight dislocations in anisotropic materials using simplified anisotropic first strain gradient elasticity. This theory is a simplification of Mindlin's anisotropic first strain gradient elasticity theory based on the key intuition that it is possible to approximate the anisotropy of the constitutive tensor of rank six, $\mathbb{D}_{ijmkln}$, as given in Eq. (11) because the classical anisotropy of the constitutive tensor of rank four, $\mathbb{C}_{ijkl}$, is dominant even within the defects core region. In other words, the theory

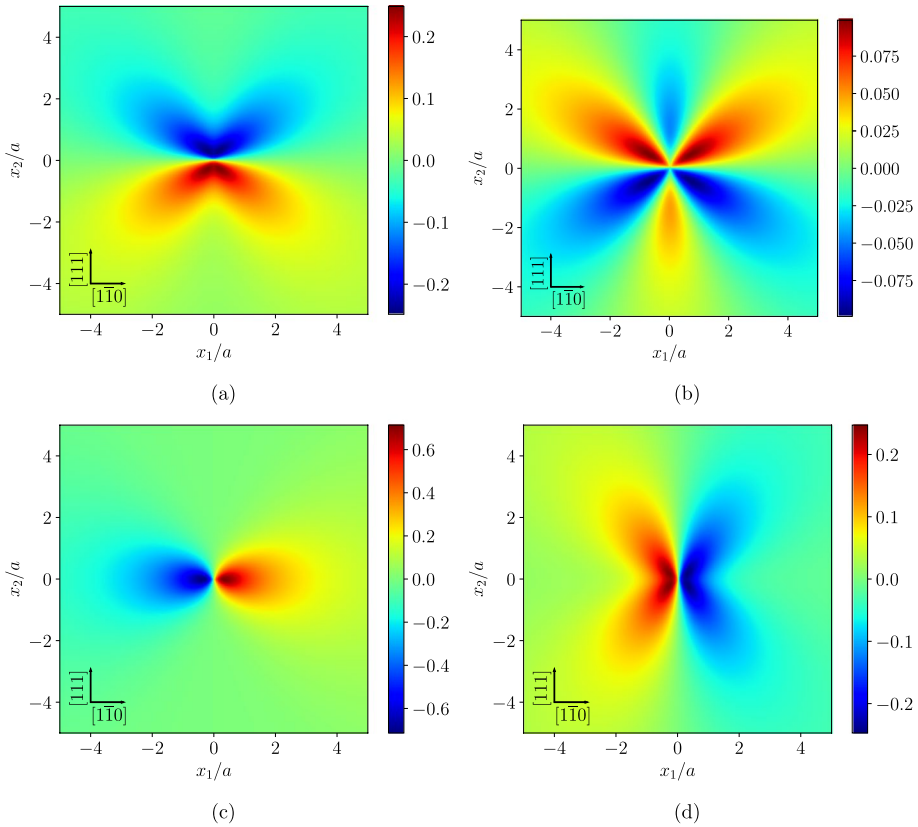

Fig. 21 Non-singular elastic distortion components of an edge dislocation in fcc Al: **a** β_{xx}, **b** β_{yy}, **c** β_{xy}, **d** β_{yx}

approximates the gradient anisotropy and retains the full classical anisotropy. We showed in previous work that this is an excellent approximation, in good agreement with atomistic calculations without any fitting constant (see, e.g., Po et al. (2018)). In the framework of simplified anisotropic first strain gradient elasticity, all necessary Green tensor functions, being non-singular, are derived. Interesting to note that the two-dimensional Green tensor of the twofold anisotropic Helmholtz-Navier operator is given as sum of a classical part and a part given in terms of a Meijer *G*-function. For generalized plane strain of dislocations, the two-dimensional dislocation key-equations (anisotropic Mura-Willis-like equation for the non-singular elastic distortion tensor, anisotropic Burgers-like equation for the non-singular displacement vector, anisotropic Blin's-like formula for the elastic strain energy, anisotropic Peach-Koehler-like stress equation, Peach-Koehler force) have been derived in terms of two-dimensional Green tensor of the twofold anisotropic Helmholtz-Navier operator. Furthermore, the two-dimensional dislocation key-equations are specified to straight dislocations in anisotropic media and, in particular, in cubic crystals. All relevant material parameters are computed for bcc and fcc cubic crystals such as iron (Fe), tungsten (W), copper (Cu) and aluminum (Al) from a second nearest-neighbour modified embedded-atom-method (2NN MEAM) interatomic potential. As representative application, the elastic distortion

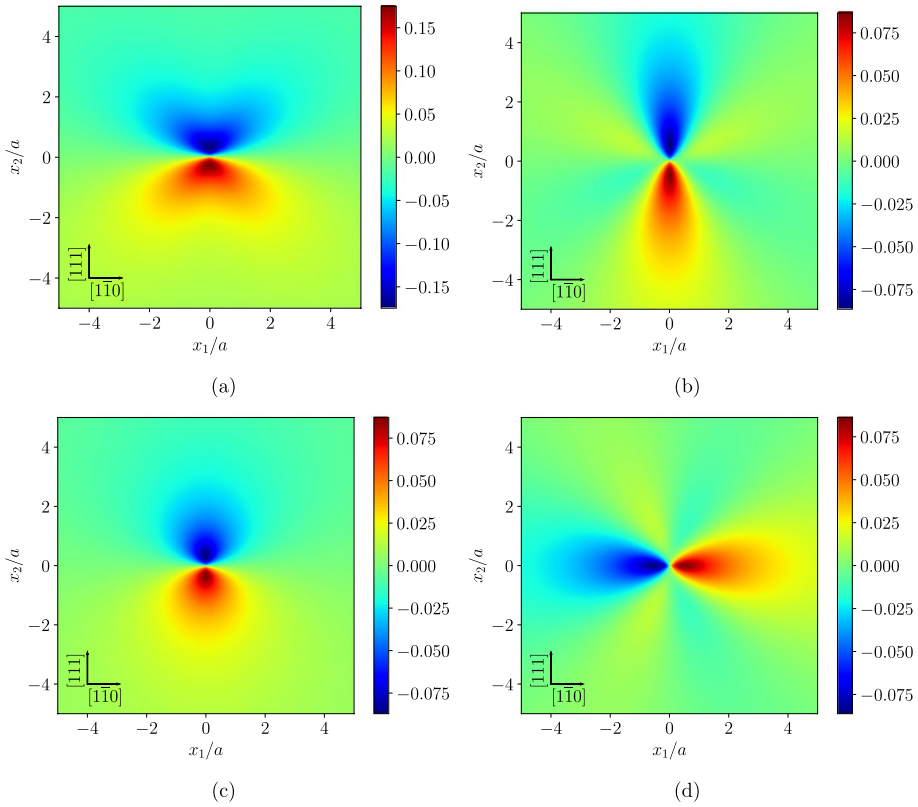

Fig. 22 Non-singular stress components of an edge dislocation in fcc Al in units of eV/Å^3: **a** σ_{xx}, **b** σ_{yy}, **c** σ_{zz}, **d** σ_{xy}

and stress fields of screw and edge dislocations of $\frac{1}{2}\langle 111\rangle$ Burgers vector in bcc iron and bcc tungsten and screw and edge dislocations of $\frac{1}{2}\langle 110\rangle$ Burgers vector in fcc copper and fcc aluminum have been computed and presented in contour plots, showing that the obtained dislocation fields are non-singular.

Appendix A: Simplified anisotropic strain gradient elasticity for cubic crystals

For cubic crystals, the simplified anisotropic strain gradient elasticity can be obtained from Mindlin's anisotropic strain gradient elasticity as special case if we assume the following values for the gradient-elastic constants

$$\begin{aligned} &a_1 = 0\,, \quad a_2 = \frac{C_{12}\,\ell^2}{2}\,, \quad a_3 = 0\,, \quad a_4 = C_{44}\,\ell^2\,, \quad a_5 = 0\,, \\ &a_6 = 0\,, \quad a_7 = 0\,, \quad a_8 = (C_{11} - C_{12} - 2C_{44})\,\ell^2\,, \; a_9 = 0\,, \; a_{10} = 0\,, \\ &a_{11} = 0\,. \end{aligned} \tag{109}$$

Using the relations (109), the constitutive tensor of rank six, Eq. (103), reduces to

$$\mathbb{D}_{ijmkln} = \ell^2\,\delta_{mn}\big[C_{12}\,\delta_{ij}\delta_{kl} + C_{44}\,\big(\delta_{il}\delta_{jk} + \delta_{ik}\delta_{jl}\big) + (C_{11} - C_{12} - 2C_{44})\delta_{ijkl}\big] \tag{110}$$

and the double stress tensor (14) becomes

$$\tau_{ijm} = \ell^2\big[C_{12}\,\delta_{ij}\partial_m e_{ll} + 2C_{12}\,\partial_m e_{ij} + (C_{11} - C_{12} - 2C_{44})\delta_{ijkl}\partial_m e_{kl}\big]\,. \tag{111}$$

It is worth noting that the double stress tensor (111) is nothing but the gradient of the Cauchy stress tensor (13) with one length scale parameter ℓ. The double stress tensor (111) is much simpler than the expression of the double stress tensor for cubic crystals in Mindlin's anisotropic strain gradient elasticity theory (see Lazar et al. (2022)). In this way, simplified anisotropic strain gradient elasticity has the meaning of an effective and robuste generalized continuum theory with approximate symmetry for non-singular dislocations.

Acknowledgements
Markus Lazar gratefully acknowledges the grant from the Deutsche Forschungsgemeinschaft (Grant number LA1974/4-2).

Authors' contributions
M.L. wrote the main manuscript. G.P. prepared the figures 5-20. All authors reviewed the manuscript.

Funding
Open Access funding enabled and organized by Projekt DEAL. This work was funded by the Deutsche Forschungsgemeinschaft (DFG, German Research Foundation) under project LA1974/4-2.

Availability of data and materials
No datasets were generated or analysed during the current study.

Declarations

Competing interests
The authors declare no competing interests.

Received: 18 November 2023 Accepted: 27 February 2024
Published: 26 March 2024

References

N.C. Admal, J. Marian, G. Po, The atomistic representation of first strain-gradient elastic tensors. J. Mech. Phys. Solids **99**, 93–115 (2017)
B.C. Altan, E.C. Aifantis, On some aspects in the special theory of gradient elasticity. J. Mech. Behav. Mater. **8**, 231–282 (1997)
R.J. Asaro, J.P. Hirth, D.M. Barnett, J. Lothe, A further synthesis of sextic and integral theories for dislocations and line forces in anisotropic media. Phys. Status Solidi (b) **60**, 261–271 (1973)
N. Auffray, H. Le Quang, Q.C. He, Matrix representations for 3D strain-gradient elasticity. J. Mech. Phys. Solids **61**, 1202–1223 (2013)
D.J. Bacon, D.M. Barnett, R.O. Scattergood, Anisotropic continuum theory of defects. Prog. Mater. Sci. **23**, 51–262 (1980)
R.W. Balluffi, *Introduction to Elasticity Theory for Crystal Defects* (Cambridge University Press, Cambridge, 2012)
D.M. Barnett, L.A. Swanger, The elastic energy of a straight dislocation in an infinite anisotropic elastic medium. Phys. Status Solidi (b) **48**, 419–428 (1971)
D.M. Barnett, J. Lothe, Synthesis of the sextic and the integral formalism for dislocations, Green's function and structure waves in anisotropic elastic solids. Phys. Nor. **7**, 13–19 (1973)
J. Baštecká, Dislocation stress fields in α-Fe. Czechoslov. J. Phys. **15**, 595–601 (1965)
Y. Cui, G. Po, Y.P. Pellegrini, M. Lazar, N. Ghoniem, Computational 3-dimensional dislocation elastodynamics. J. Mech. Phys. Solids **126**, 20–51 (2019)
P.H. Dederichs, G. Leibfried, Elastic Green's function for anisotropic cubic crystals. Phys. Rev. **188**, 1175–1183 (1969)
M.R. Delfani, E. Tavakol, Uniformly moving screw dislocation in strain gradient elasticity. European Journal of Mechanics-A/Solids **73**, 349–355 (2019)
M.R. Delfani, S. Taaghi, E. Tavakol, Uniform motion of an edge dislocation within Mindlin's first strain gradient elasticity. Int. J. Mech. Sci. **179**, 105701 (2020)
R. deWit, Theory of disclinations II. J. Res. Natl. Bur. Stand. **77A**, 49–100 (1973a)
R. deWit, Theory of disclinations IV. J. Res. Natl. Bur. Stand. **77A**, 607–658 (1973b)
A.C. Eringen, in *Nonlinear Equations in Physics and Mathematics*, ed. by A.O. Barut. Nonlocal continuum mechanics and some applications (D. Reidel Publishing Company, Dordrecht, 1978), pp. 271–318
A.C. Eringen, *Nonlocal Continuum Field Theories* (Springer, New York, 2002)
A. Erdélyi, W. Magnus, F. Oberhettinger, F.G. Tricomi, in *Higher Transcendental Functions*. "Definition of the *G*-Function" sections 5.3–5.6, vol 1 (Krieger, New York, 1981), pp. 206–222
I.M. Gitman, H. Askes, E. Kuhl, E.C. Aifantis, Stress concentrations in fractured compact bone simulated with a special class of anisotropic gradient elasticity. Int. J. Solids Struct. **47**, 1099–1107 (2010)
I.S. Gradshteyn, I.M. Ryzhik, in *Tables of Integrals, Series, and Products*, 6th edn. "Meijer's and MacRobert's Function (*G* and *E*)" and "Meijer's *G*-Function" sections 7.8 and 9.3 (Academic Press, San Diego, 2000), pp. 843–850 and 1022–1025
MYu. Gutkin, E.C. Aifantis, Screw dislocation in gradient elasticity. Scr. Mater. **35**, 1353–1358 (1996)

MYu. Gutkin, E.C. Aifantis, Edge dislocation in gradient elasticity. Scr. Mater. **36**, 129–135 (1997)
C.S. Hartley, Y. Mishin, Characterization and visualization of the lattice misfit associated with dislocation cores. Acta Matererialia **53**, 1313–1321 (2005)
J.P. Hirth, J. Lothe, *Theory of Dislocations*, 2nd edn. (Wiley, New York, 1982)
H.O.K. Kirchner, in *Dislocation 1984*, ed. by P. Veyssière, L. Kubin, J. Castaing. The concept of the line tension: theory and experiments (Editions du CNRS, Paris, 1984), pp. 53–71
A.M. Kosevich, in *Dislocations in Solids, Vol. I. The elastic theory*, ed. by F.R.N. Nabarro. Crystal dislocations and the theory of elasticity. (North-Holland Publishing company Amsterdam, New York, Oxford, 1979), pp. 33–141
S. Kret, P. Dłużewski, P. Dłużewski, W. Sobczak, Measurement of the dislocation core distribution by digital processing of high transmission electron microscopy micrographs: a new technique for studying defects. J Phys. Cond. Matter **12**, 10313–10318 (2000)
E. Kröner, *Kontinuumstheorie der Versetzungen und Eigenspannungen* (Springer, Berlin, 1958)
R.W. Lardner, Dislocations in materials with couple stress. IMA J. Appl. Math. **7**, 126–137 (1971)
M. Lazar, Non-singular dislocation loops in gradient elasticity. Phys. Lett. A **376**, 1757–1758 (2012)
M. Lazar, The fundamentals of non-singular dislocations in the theory of gradient elasticity: Dislocation loops and straight dislocations. Int. J. Solids Struct. **50**, 352–362 (2013)
M. Lazar, On gradient field theories: gradient magnetostatics and gradient elasticity. Philos. Mag. **94**, 2840–2874 (2014)
M. Lazar, Irreducible decomposition of strain gradient tensor in isotropic strain gradient elasticity. Z. Angew. Math. Mech. (ZAMM) **96**, 1291–1305 (2016)
M. Lazar, Non-singular dislocation continuum theories: Strain gradient elasticity versus Peierls-Nabarro model. Philos. Mag. **97**, 3246–3275 (2017)
M. Lazar, Displacements and stress functions of straight dislocations and line forces in anisotropic elasticity: A new derivation and its relation to the integral formalism. Symmetry **13**(9), 1721 (2021)
M. Lazar, Reduced strain gradient elasticity model with two characteristic lengths: fundamentals and application to straight dislocations. Contin. Mech. Thermodyn. **34**, 1433–1454 (2022)
M. Lazar, E. Agiasofitou, Screw dislocation in nonlocal anisotropic elasticity. Int. J. Eng. Sci. **49**, 1404–1414 (2011)
M. Lazar, E. Agiasofitou, Toupin-Mindlin first strain-gradient elasticity for cubic and isotropic materials at small scales. Proc. Appl. Math. Mech. **23**, e202300121 (2023)
M. Lazar, E. Agiasofitou, T. Böhlke, Mathematical modeling of the elastic properties of cubic crystals at small scales based on the Toupin-Mindlin anisotropic first strain gradient elasticity. Contin. Mech. Thermodyn. **34**, 107–136 (2022)
M. Lazar, E. Agiasofitou, G. Po, Three-dimensional nonlocal anisotropic elasticity: a generalized continuum theory of Ångström-mechanics. Acta Mech. **231**, 743–781 (2020)
M. Lazar, H.O.K. Kirchner, The Eshelby stress tensor, angular momentum tensor and dilatation flux in gradient elasticity. Int. J. Solids Struct. **44**, 2477–2486 (2007)
M. Lazar, H.O.K. Kirchner, Generalised plane strain embedded in three-dimensional anisotropic elasticity. Philos. Mag. **101**, 2584–2598 (2021)
M. Lazar, H.O.K. Kirchner, Dislocation loops in anisotropic elasticity: displacement field, stress function tensor and interaction energy. Philos. Mag. **93**, 174–185 (2013)
M. Lazar, G.A. Maugin, Nonsingular stress and strain fields of dislocations and disclinations in first strain gradient elasticity. Int. J. Eng. Sci. **43**, 1157–1184 (2005)
M. Lazar, G.A. Maugin, E.C. Aifantis, On dislocations in a special class of generalized elasticity. Phys. Status Solidi (b) **242**, 2365–2390 (2005)
M. Lazar, G. Po, The solid angle and the Burgers formula in the theory of gradient elasticity: Line integral representation. Phys. Lett. A **378**, 597–601 (2014)
M. Lazar, G. Po, The non-singular Green tensor of gradient anisotropic elasticity of Helmholtz type. Eur. J. Mech. A Solids **50**, 152–162 (2015a)
M. Lazar, G. Po, The non-singular Green tensor of Mindlin's anisotropic gradient elasticity with separable weak nonlocality. Phys. Lett. A **379**, 1538–1543 (2015b)
M. Lazar, G. Po, Singularity-free dislocation continuum theory for anisotropic crystals. Proc. Appl. Math. Mech. **18**, e201800095 (2018a)
M. Lazar, G. Po, On Mindlin's isotropic strain gradient elasticity: Green tensors, regularization, and operator-split. J. Micromech. Mol. Phys. **3**, 1840008 (2018b)
R.D. Mindlin, Micro-structure in linear elasticity. Arch. Ration. Mech. Anal. **16**, 51–78 (1964)
R.D. Mindlin, in *Mechanics of Generalized Continua, IUTAM Symposium*, ed. by E. Kröner. Theories of elastic continua and crystal lattice theories (Springer, Berlin, 1968), pp. 312–320
R.D. Mindlin, Elasticity, piezoelectricity and crystal lattice dynamics. J. Elast. **2**, 217–282 (1972)
MODEL (2014). https://github.com/giacomo-po/MoDELib
T. Mura, *Micromechanics of Defects in Solids*, 2nd edn. (Martinus Nijhoff, Dordrecht, 1987)
G. Po, N.C. Admal, M. Lazar, The Green tensor of Mindlin's anisotropic first strain gradient elasticity. Mater. Theory **3**, 3 (2019)
G. Po, M. Lazar, N.C. Admal, N. Ghoniem, A non-singular theory of dislocations in anisotropic crystals. Int. J. Plast. **103**, 1–22 (2018)
G. Po, M. Lazar, D. Seif, N. Ghoniem, Singularity-free dislocation dynamics with strain gradient elasticity. J. Mech. Phys. Solids **68**, 161–178 (2014)
C. Polizzotto, Anisotropy in strain gradient elasticity: Simplified models with different forms of internal length and moduli tensors. Eur. J. Mech. A **71**, 51–63 (2018)
D. Rogula, Some basic solutions in strain gradient elasticity theory of an arbitrary order. Arch. Mech. **25**, 43–68 (1973)
D. Seif, G. Po, M. Mrovec, M. Lazar, C. Elsässer, P. Gumbsch, Atomistically enabled nonsingular anisotropic elastic representation of near-core dislocation stress fields in α-iron. Phys. Rev. B **91**, 184102 (2015)

H.M. Shodja, H. Moosavian, F. Ojaghnezhad, Toupin-Mindlin first strain gradient theory revisited for cubic crystals of hexoctahedral class: analytical expression of the material parameters in terms of the atomic force constants and evaluation via ab initio DFT. Mech. Mater. **123**, 19–29 (2018)
J.W. Steeds, *Introduction to anisotropic elasticity theory of dislocations* (Clarendon Press, Oxford, 1973)
A.N. Stroh, Dislocations and cracks in anisotropic elasticity. Philos. Mag. **3**, 625–646 (1958)
A.N. Stroh, Steady state problems in anisotropic elasticity. J. Math. Phys. **41**, 77–103 (1962)
V. Taupin, L. Capolungo, C. Fressengeas, Disclination mediated plasticity in shear-coupled boundary migration. Int. J. Plast. **53**, 179–192 (2014)
V. Taupin, L. Capolungo, C. Fressengeas, Nonlocal elasticity tensors in dislocation and disclination cores. J. Mech. Phys. Solids **100**, 62–84 (2017)
C. Teodosiu, *Elastic Models of Crystal Defects* (Springer-Verlag, Berlin, 1982)
T.C.T. Ting, *Anisotropic Elasticity* (Oxford Science Publishers, Oxford, 1996)
A. Vattré, E. Pan, Semicoherent heterophase interfaces with core-spreading dislocation structures in magneto-electro-elastic multilayers under external surface loads. J. Mech. Phys. Solids **124**, 929–956 (2019)
V.S. Vladimirov, *Equations of Mathematical Physics* (Marcel Dekker Inc, New York, 1971)
W.A. Wooster, *Tensors and Group Theory for the Physical Properties of Crystals* (Oxford University Press, Oxford, 1973)
M.H. Yoo, B.T.M. Loh, Characteristics of stress and dilatation fields of straight dislocations in anisotropic crystals. J. Appl. Phys. **41**, 2805–2814 (1970)
M.H. Yoo, B.T.M. Loh, Numerical calculation of elastic properties for straight dislocations in anisotropic crystals. United States. p. 1971. https://doi.org/10.2172/4008219
Y. Zhang, J. Liu, H. Chu, J. Wang, Elastic fields of a core-spreading dislocation in anisotropic bimaterials. Int. J. Plast. **81**, 231–248 (2016)

Publisher's Note